



## A robust blind color image watermarking in quaternion Fourier transform domain

Wang Xiang-yang<sup>a,b,\*</sup>, Wang Chun-peng<sup>a</sup>, Yang Hong-ying<sup>a</sup>, Niu Pan-pan<sup>a</sup>

<sup>a</sup> School of Computer and Information Technology, Liaoning Normal University, Dalian 116029, China

<sup>b</sup> State Key Laboratory of Information Security, Institute of Software, Chinese Academy of Sciences, Beijing 100190, China

### ARTICLE INFO

#### Article history:

Received 8 November 2011

Received in revised form 5 August 2012

Accepted 5 August 2012

Available online 24 August 2012

#### Keywords:

Color image watermarking

Color attack

Geometric distortion

Quaternion Fourier transform

Least squares support vector machine

### ABSTRACT

Most of the existing color image watermarking schemes were designed to mark the image luminance component only, which have some disadvantages: (i) they are sensitive to color attacks because of ignoring the correlation between different color channels, (ii) they are always not robust to geometric distortions for neglecting the watermark desynchronization. It is a challenging work to design a robust color image watermarking scheme. Based on quaternion Fourier transform and least squares support vector machine (LS-SVM), we propose a robust blind color image watermarking in quaternion Fourier transform domain, which has good visual quality. Firstly, the original color image is divided into color image blocks. Then, the fast quaternion Fourier transform is performed on the color image block. Finally, the digital watermark is embedded into original color image by adaptively modulating the real quaternion Fourier transform coefficients of color image block. For watermark decoding, the LS-SVM correction with pseudo-Zernike moments is utilized. Experimental results show that the proposed color image watermarking is not only robust against common image processing operations such as filtering, JPEG compression, histogram equalization, and image blurring, but also robust against the geometrical distortions.

© 2012 Elsevier Inc. All rights reserved.

## 1. Introduction

Because of the rapid advance of network technology, humans can arbitrarily and easily access or distribute any multimedia data from networks. Hence, the protection of intellectual property becomes more and more attentive and important for the society. Based on this scheme, many methods are being developed (Cheddad et al., 2010; Huang et al., 2010). Digital watermarking is a favorable method for copyright protection of multimedia. It is a digital code embedded in the host data and typically contains information about origin, status, and/or destination of the data. A digital watermark is an identification code that carries information about the copyright owner, the creator of the work, the authorized consumer, etc. It is permanently embedded into the digital data for copyright protection and may be used to check whether the data have been illegally modified (Cheddad et al., 2010; Huang et al., 2010). For different purposes, digital watermarking has been branched into two classifications: robust watermarking technique and fragile watermarking technique. Robust digital watermarking is used to protect ownership of the digital media. In contrast, the

purpose of fragile watermarking technique is digital media authentication, that is, to ensure the integrity of the digital media.

In the last decade, there has been an unprecedented development in the robust image watermarking field. On the other hand, attacks against image watermarking systems have become more sophisticated (Kumar and Santhi, 2011; Sadasivam et al., 2011). In general, these attacks on watermarking systems can be categorized into noise-like common image processing operations and geometric distortions. While the noise-like common image processing operations, such as lossy compression, noise addition, histogram equalization, and light increasing, reduces watermark energy, geometric distortions can induce synchronization errors between the extracted watermark and the original watermark during the detection, even though the watermark still exists in the watermarked image.

According to quaternion Fourier transform and least squares support vector machine (LS-SVM), a robust blind color image watermarking in quaternion Fourier transform domain is proposed, which has good visual quality. Firstly, the original color image is divided into color image blocks. Then, the fast quaternion Fourier transform is performed on the color image block. Finally, the digital watermark is embedded into original color image by adaptively modulating the real quaternion Fourier transform coefficients of color image block. The main steps of digital watermark detecting procedure include: (1) fast quaternion Fourier transform is performed on the training images, which produces a real coefficient matrix and three imaginary coefficient matrices, (2) some

\* Corresponding author at: School of Computer and Information Technology, Liaoning Normal University, Dalian 116029, China. Tel.: +86 0411 85992415; fax: +86 0411 82158365.

E-mail address: [wxy37@126.com](mailto:wxy37@126.com) (X.-y. Wang).

low-order pseudo-Zernike moments of the real coefficient matrix are computed, which are regarded as the effective feature vectors, (3) the appropriate kernel function is selected for training, and a LS-SVM training model can be obtained, (4) the watermarked color image is corrected with the well trained LS-SVM model, and (5) the digital watermark is extracted from the corrected watermarked color image. The experimental results show the outstanding robustness of the proposed scheme against different common image processing operations and geometrical distortions.

The rest of this paper is organized as follows. A review of previous related work is presented in Section 2. Section 3 describes the fast quaternion Fourier transform of color images. Section 4 introduces basic theory about LS-SVM. Section 5 contains the description of our watermark embedding procedure. Section 6 covers the details of the watermark detection procedure. Simulation results in Section 7 will show the performance of our scheme. Finally, Section 8 concludes this presentation.

## 2. Related work

Nowadays, several approaches that counterattack geometric distortions have been developed. These schemes can be roughly divided into exhaustive search, invariant transform, geometrical correction, and feature-based algorithms (Kumar and Santhi, 2011; Zheng et al., 2007; Muhammad, 2011).

**Exhaustive search:** The simplest method for watermark detection after geometric distortions is an exhaustive search. This approach consists simply in inverting each hypothetical geometric deformation that might have been applied to the watermarked image, and then applying the watermark detector once for each possible distortion parameter. Obviously, this method is feasible for a restricted number of hypothetical deformations (e.g., scaling, rotation, translation), but it rapidly becomes intractable as the number of possible distortions increases. Furthermore, it tends to largely increase the false positive probability (Muhammad, 2011; Valizadeh and Wang, 2011).

**Invariant transform:** Another solution consists in embedding the watermark in a geometrical invariant subspace. In Jung et al. (2011), Kang et al. (2010), Wang and Hou (2010) and Rastegar et al. (2011), the watermark was embedded in an affine-invariant domain by using Fourier-Mellin transform, generalized Radon transform, geometric moments, singular value, and histogram shape respectively. Zhang et al. (2011) proposed a new watermarking approach which allows watermark detection and extraction under affine transformation attacks. The novelty of the approach stands on a set of affine invariants derived from Legendre moments. Watermark embedding and detection are directly performed on this set of invariants. These moments can be exploited for estimating the geometric distortion parameters in order to permit watermark extraction. In practice, this solution can be implemented for simple affine transformations, but it is inapplicable as soon as the image undergoes local geometrical deformations. Moreover, problems of approximation due to the discrete nature of the images, plus the reduction of the embedding space make the watermark weakly resistant to low-pass filtering and lossy compression.

**Geometrical correction:** Template correction is one of the most common resynchronization techniques, in which an additional watermark or template is inserted into the host image. Basically, this template is used as a reference to detect and compensate for geometrical deformations such as affine transforms. By focusing on a simple example, Barni (2005) investigated the effectiveness of exhaustive watermark detection and resynchronization through template matching against geometric distortions. Liu et al. (2007) presents an image rectification scheme that can be used by any image watermarking algorithm to provide robustness

against rotation, scaling and translation (RST). In the watermarking, a small block is cut from the log-polar mapping (LPM) domain as a matching template, and a new filtering method is proposed to compute the cross-correlation between this template and the magnitude of the LPM of the image having undergone RST transformations to detect the rotation and scaling parameters. Qiu et al. (2011) proposed a robust image watermarking scheme. The scheme is composed of two parts: non-informative watermark embedded in b component of Lab color space, which is used to recover embedded region from the modified image; Informative watermark embedded in DCT domain that carries information can be used to protect copyright. This scheme is a blind watermarking scheme, extraction can be proposed without the presence of original image. In scheme (Kaur and Kaur, 2009), a watermarking technique is suggested that incorporates two watermarks in a host image for improved robustness. A watermark, in form of a PN sequence (information watermark), is embedded in the DCT domain of the cover image. The second watermark (synchronization template) is embedded in the already watermarked image. Synchronization template does not contain any information and is used only to detect and correct any geometrical changes came after the attack on the image. One major advantage of template corrections is their effectiveness to address synchronization of affine transformations, but this kind of pattern is unfortunately, for both watermarker and attacker, easily detectable in frequency domain. It is then relatively easy for a malicious party to remove these peaks, thus depriving the detector of any means of resynchronization.

Recently, some new geometrical corrections are introduced to the image watermarking domain. Liu and Huang (2008) presented a new robust watermarking scheme for color image by using scale invariant features transform image correction. In order to detect digital watermark, the scale invariant features of images are firstly extracted, and the match points between the watermarking image and the reference image are found. Then the watermarking image is corrected by affine transform of these match points. In approach (Nian et al., 2010), a definition of weight Hausdorff distance is defined. It is applied to evaluate the similarity between original and geometric distorted watermarking image. A fast divide and conquer strategy in six dimension is used to search the transformation parameters. The geometric distortion is corrected by the parameters. As a result, a distorted watermarking image could be corrected based on image feature. Wang et al. (2009) proposed a robust image watermarking detection algorithm against geometric distortions, in which the steady Krawtchouk moments are utilized. In scheme (Wu, 2009), in order to obtain the rotation, scaling and translation (RST) parameters, the support vector machine (SVM) are utilized to learn image geometric pattern represented by six combined low order image moments. The watermark extraction is carried out after watermarked image has been synchronized without original image.

**Feature-based:** The last class of resynchronization techniques uses image content to recover the watermark after geometrical transformations. Its basic idea is that, by binding the watermark with the geometrically invariant image features, the watermark detection can be done without synchronization error. Seo and Yoo (2006) introduce a content-based image watermarking algorithm based on scale-space representation. Gao et al. (2010) proposed a new image watermarking scheme on the basis of Seo's work (Seo and Yoo, 2006), which is insensitive to geometric distortions as well as common image processing operations. Wang et al. (2007) presented a feature-based digital image watermarking scheme in DFT domain. Lin et al. (2011) proposed a watermarking scheme that is robust to RST attacks, blind-detectable and has a reasonable embedding capacity. By embedding the message in the RST-invariant features of the image and introducing an human visible system (HVS)-based watermark embedding

strategy, the message can still be preserved well in salient points even if the image is destroyed by severe attacks, for instance, rotation, scaling, and translation. Deng et al. (2009) gives a content-based watermarking scheme that combines the invariant feature extraction with watermark embedding by using moments. Based on multi-scale SIFT (Scale Invariant Feature Transform) detector and local image histogram shape invariance, Wang et al. (2011) proposed a content based image watermarking algorithm with good visual quality and reasonable resistance toward desynchronization attacks. Li et al. (2011) introduced a novel feature point based image watermarking scheme to achieve high capacity information hiding and generalized watermark robustness. The key idea is to embed a binary watermark image into multi-scale feature point based local characteristic regions in transform domain. To further reduce the computational complexity and exploit the statistical characteristics which are independent of the position of pixels in the image plane, Deng and Gao (2010) proposed a geometrically resistant image watermarking approach by using local histogram. Tsai et al. (2011) proposed a feature region selection method based on the idea of simulated attacking and multidimensional knapsack problem (MDKP) optimization techniques. This method can be integrated into the feature-based watermarking schemes to enhance their robustness against various types of attack. It is not difficult to see that the feature-based approaches are better than others in terms of robustness. However, some drawbacks indwelled in current feature-based schemes restrict the performance of watermarking system. First, the feature point extraction is sensitive to image modification. Second, the computational complexity in calculating the features of an image before watermark detection is added. Third, the capacity of watermark data is small.

Most of the existing watermarking schemes mentioned before were designed to mark grayscale images. However, color image is more common in our everyday life, and can provide more information than grayscale image, so it is very important to embed the digital watermark into color image for copyright protection. With the introduction of color imaging, some of early grayscale watermarking techniques have been extended to color images. Fu and Shen (2008) presented an oblivious color image watermarking scheme based on Linear Discriminant Analysis (LDA). The watermark accompanied with a reference is embedded into the RGB channels of color images. By applying the embedded reference watermark, a linear discriminant matrix is obtained. The watermark can be correctly extracted under several different attacks. Liu (2010) presented a wavelet-based watermarking scheme for color images. The watermarking scheme is based on the design of a color visual model, which is the modification of a perceptual model used in the image coding of gray scale images. The model is to estimate the noise detection threshold of each wavelet coefficient in luminance and chrominance components of color images in order to satisfy transparency and robustness required by the color image watermarking technique. Unfortunately, the approach is non-invariant to image rotation and translation attacks. Zheng and Feng (2009) proposed a color watermarking scheme based on the multi-channel framework, which generates a watermarking template from one of image channels data, and then embeds this watermarking template into another image channel. Fındık et al. (2011) suggested a watermarking technique that uses artificial immune recognition system to protect color image's intellectual property rights. The watermark is embedded in the blue channel of a color image. M-bit binary sequence embedded into the color image is used to train artificial immune recognition system. With this composed technique, extracting the watermark which is embedded into the color image is carried out using artificial immune recognition system. Dejey and Rajesh (2011) introduced two color image watermarking using the combined discrete wavelet transform-fan

beam transform (DWT-FBT). The two schemes proposed in the combined domain are (i) wavelet fan beam watermarking on luminance and chrominance and (ii) wavelet fan beam watermarking on chrominance alone. Tsai and Sun (2007) proposed a watermarking technique called SVM-based color image watermarking (SCIW) for the authentication of color images. The SCIW method utilizes the set of training patterns to train the SVM and then applies the trained SVM to classify a set of testing patterns. Following the results produced by the classifier, the SCIW method retrieves the hidden watermark without the original image during watermark extraction. Peng et al. (2010) presented a color image watermarking method in multiwavelet domain based on support vector machines (SVMs), in which the special frequency band and property of image in multiwavelet domain are employed. Niu et al. (2011) described a blind color image watermarking algorithm by using the support vector regression (SVR) and nonsubsampled contourlet transform (NSCT). Hazem and Sulaiman (2011) proposed a wavelet-based blind technique for color image watermarking by using self-embedded color permissibility (CIW-SECP). The CIW-SECP technique is based on embedding two watermarks in a spread-spectrum fashion in the U and V planes of the YUV color space. Tsui et al. (2008) proposed a nonblind color image watermarking method, which requires the original image for watermark extraction. The method encodes the  $L^*a^*b^*$  components of color images and watermarks are embedded as vectors in the frequency domain of the channels by using the quaternion Fourier transform. But, it suffers from its lower visual quality because of ignoring pure quaternion representation. In addition, it is very fragile to some geometric distortions. Chou and Liu (2010) proposed a color image watermarking scheme, which is perceptually optimized by embedding high-strength watermark signals in wavelet coefficients of high perceptual redundancy. The strength of the embedded watermark signal is determined by the amount of perceptual redundancy inherent in the corresponding wavelet coefficient. Singhal et al. (2011) presented a comparative study of various wavelet techniques for color image watermarking and tested the results in terms of watermarked image quality, extracted watermark quality and its substance to JPEG 2000 compression. The above-mentioned color image watermarking schemes were designed mainly to mark the image luminance component only, which have some disadvantages in varying degrees: (i) they are sensitive to color attacks because of ignoring the correlation between different color channels (Benhocine et al., 2008), (ii) they are always not robust to geometric distortions for neglecting the watermark desynchronization.

### 3. Fast quaternion Fourier transform of color images

In this section, we describe the fast quaternion Fourier transform of color images. We first introduce the quaternion representation of images. Next we discuss the fast quaternion Fourier transform of color images.

#### 3.1. The quaternion representation of color images

The quaternion, which is a type of hypercomplex number, was formally introduced by Hamilton in 1843 (Moxey et al., 2002). It is a generalization of complex number. The quaternion can be represented as a four-dimensional complex number with one real part and three imaginary parts as follows:

$$q = w + xi + yj + zk \quad (1)$$

where  $w$ ,  $xy$  and  $z$  are real numbers, and  $i$ ,  $j$ , and  $k$  are imaginary operators presenting the following properties:

$$i^2 = j^2 = k^2 = ijk = -1$$

$$\mathbf{ij} = \mathbf{k} \cdot \mathbf{jk} = \mathbf{i} \cdot \mathbf{ki} = \mathbf{j}$$

$$\mathbf{ji} = -\mathbf{k} \cdot \mathbf{kj} = -\mathbf{i} \cdot \mathbf{ik} = -\mathbf{j}$$

Color image pixels have three components, and they can be represented in quaternion form using pure quaternions. For example, a pixel at image coordinates  $(m, n)$  in an RGB image can be represented as

$$f(m, n) = R(m, n)\mathbf{i} + G(m, n)\mathbf{j} + B(m, n)\mathbf{k} \quad (2)$$

where  $R(m, n)$  is the red component, and  $G(m, n)$  and  $B(m, n)$  are the green and blue components of the pixel, respectively.

The same approach may be used with a luminance-chrominance color space, such as  $YC_bC_r$ . The choice of the imaginary part to represent pixel values is determined by interpretation of color pixels as vectors. The imaginary part of a quaternion has three components and may also be associated with a 3-space vector. This choice is not arbitrary, nor is it coincidental. One interpretation of a full quaternion is that it is the ratio of two vectors, that is, the quantity that multiples one vector to give another. This is a useful geometric interpretation that is exploited in the design of color image filters.

The representation of color image pixels by pure quaternions has been conceived, and used for color image compression algorithms, color images registration, color image smoothing, and edge detection (Moxey et al., 2002; Todd and Stephen, 2007).

### 3.2. The fast quaternion Fourier transform of color images

Quaternion Fourier transform has been described by several authors (Todd and Stephen, 2007; Pei et al., 2001). The pioneering work of Sangwine and Ell (2001) predicated all these papers and was the inspiration for Todd and Stephen (2007) and Sangwine and Ell (2001). Ell's original quaternion Fourier transform (Sangwine and Ell, 2001) was defined as follows:

$$H(jw, kv) = \int_{-\infty}^{+\infty} \int_{-\infty}^{+\infty} e^{-jw\tau} h(t, \tau) e^{-kv\tau} dt d\tau \quad (3)$$

with inverse defined as

$$h(t, \tau) = \int_{-\infty}^{+\infty} \int_{-\infty}^{+\infty} e^{jw\tau} H(jw, kv) e^{kv\tau} dv dw \quad (4)$$

In 1996, Sangwine was the first to demonstrate the applicability of a quaternion Fourier transform to color images. However, subsequent attempts to implement convolution and correlation using a simple generalization of the standard complex operational formulae failed, and this motivated the search for alternate formulations of quaternion Fourier transforms. This search resulted in the following generalized quaternion Fourier transform

$$F(u, v) = \frac{1}{\sqrt{MN}} \sum_{m=0}^{M-1} \sum_{n=0}^{N-1} e^{-\mu 2\pi(\frac{mu}{M} + \frac{nv}{N})} f(m, n) \quad (5)$$

with the inverse transform defined by

$$f(m, n) = \frac{1}{\sqrt{MN}} \sum_{u=0}^{M-1} \sum_{v=0}^{N-1} e^{\mu 2\pi(\frac{mu}{M} + \frac{nv}{N})} F(u, v) \quad (6)$$

In these definitions, the quaternion operator was generalized:  $\mu$  is any unit pure quaternion. It should be noted that  $\mu^2 = -1$  (there are an infinite number of square roots of  $-1$  located on the unit sphere in three space when embedded in this fashion in quaternion four space). The operators  $i, j, k$  are now special cases of  $\mu$ , and the complex Fourier transform is a special case of this transform in which  $\mu = i$  and the function to be transformed is complex, the result  $F(v, u)$  also being complex.

Jiang et al. (2008) introduced the fast algorithms of the 2D quaternion Fourier transform by using the traditional complex fast Fourier transforms, in which each part Fourier transform is calculated by FFT algorithm by means of separating a quaternion into a real part and other imaginary parts. The fast quaternion Fourier transform of color image  $f(m, n)$  can be represented as

$$\begin{aligned} F(u, v) = & \mathbf{i}(\text{Real}(R_{RFT}) + \mu \cdot \text{Imag}(R_{RFT})) \\ & + \mathbf{j}(\text{Real}(G_{RFT}) + \mu \cdot \text{Imag}(G_{RFT})) \\ & + \mathbf{k}(\text{Real}(B_{RFT}) + \mu \cdot \text{Imag}(B_{RFT})) \end{aligned} \quad (7)$$

where  $\text{Real}(x)$  denotes the real part of complex number  $x$ ,  $\text{Imag}(x)$  denotes the imaginary part of complex number  $x$ , and  $p_{RFT}$  is the real Fourier transform of array  $p$ .

Let  $A(u, v)$  denote the real part of color image in quaternion Fourier transform domain,  $C(u, v)$ ,  $D(u, v)$ , and  $E(u, v)$  be the three imaginary parts of color image in quaternion Fourier transform domain

$$F(u, v) = A(u, v) + \mathbf{i}C(u, v) + \mathbf{j}D(u, v) + \mathbf{k}E(u, v) \quad (8)$$

The inverse fast quaternion Fourier transform of Eq. (8) can be represented as

$$\begin{aligned} f(m, n) = & (\text{Real}(A_{IRFT}) + \mu \cdot \text{Imag}(A_{IRFT})) \\ & + \mathbf{i}(\text{Real}(C_{IRFT}) + \mu \cdot \text{Imag}(C_{IRFT})) + \mathbf{j}(\text{Real}(D_{IRFT}) \\ & + \mu \cdot \text{Imag}(D_{IRFT})) + \mathbf{k}(\text{Real}(E_{IRFT}) + \mu \cdot \text{Imag}(E_{IRFT})) \end{aligned} \quad (9)$$

where  $p_{IRFT}$  is the real inverse Fourier transform of array  $p$ .

Figs. 1 and 2 show the 24-bit color images (Lena and Barbara) and their Red, Green, and Blue components. Figs. 3 and 4 show the fast quaternion Fourier transform results of 24-bit color images (Lena and Barbara).

## 4. The least squares support vector machine (LS-SVM)

Support vector machines (SVM) have been successfully applied in classification and function estimation problems after their introduction by Vapnik within the context of statistical learning theory and structural risk minimization (Vapnik, 1995). Vapnik constructed the standard SVM to separate training data into two classes. The goal of the SVM is to find the hyperplane that maximizes the minimum distance between any data point, as described in reference (Vapnik, 1995).

The standard SVM is solved using quadratic programming methods. However, these methods are often time consuming and are difficult to implement adaptively. Least squares support vector machines (LS-SVM) is capable of solving both classification and regression problems and is receiving more and more attention because it has some properties that are related to the implementation and the computational method. For example, training requires solving a set of linear equations instead of solving the quadratic programming problem involved in the original SVM. The original SVM formulation of Vapnik (1995) is modified by considering equality constraints within a form of ridge regression rather than by considering inequality constraints.

The solution follows from solving a set of linear equations instead of a quadratic programming problem. In LS-SVMs, an equality constraint-based formulation is made within the context of ridge regression as follows:

$$\begin{aligned} \min \frac{1}{2} \omega^T \omega + C \sum_{i=1}^l e_i^2 \\ \text{s.t. } y_i(\omega^T \phi(x_i) + b) = 1 - e_i, \quad i = 1, \dots, l \end{aligned} \quad (10)$$



**Fig. 1.** The 24-bit color image Lena and its red, green, and blue components: (a) original color image, (b) the red component, (c) the green component, and (d) the blue component. (For interpretation of the references to color in this figure legend, the reader is referred to the web version of the article.)

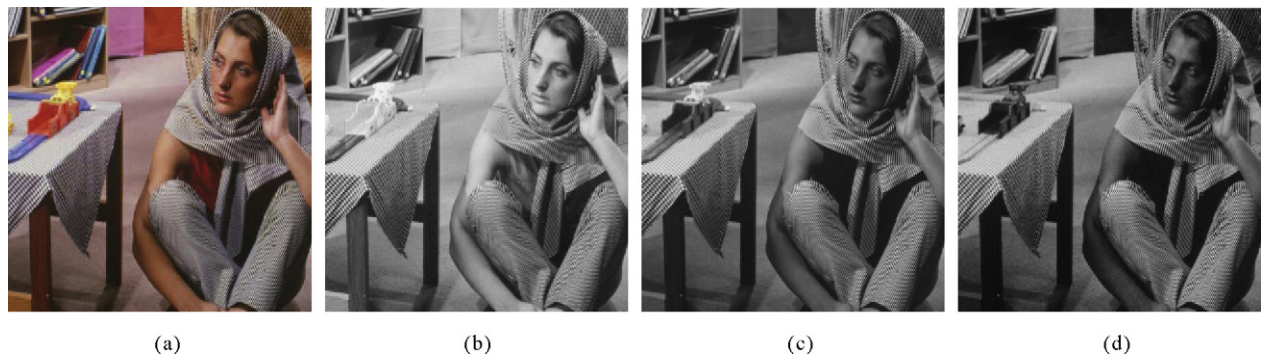


**Fig. 2.** The 24-bit color image Barbara and its red, green, and blue components: (a) original color image, (b) the red component, (c) the green component, and (d) the blue component. (For interpretation of the references to color in this figure legend, the reader is referred to the web version of the article.)

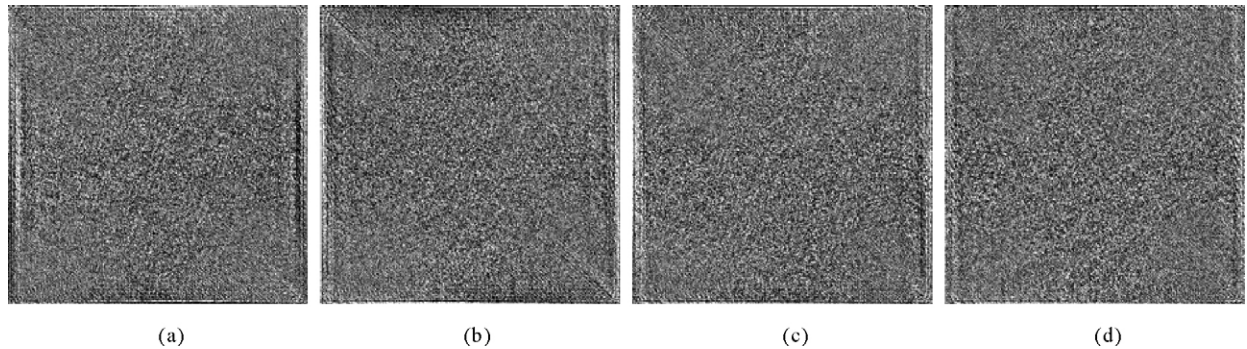


**Fig. 3.** The fast quaternion Fourier transform results of 24-bit color image Lena: (a) the real part A, (b) the imaginary part C, (c) the imaginary part D, and (d) the imaginary part E.

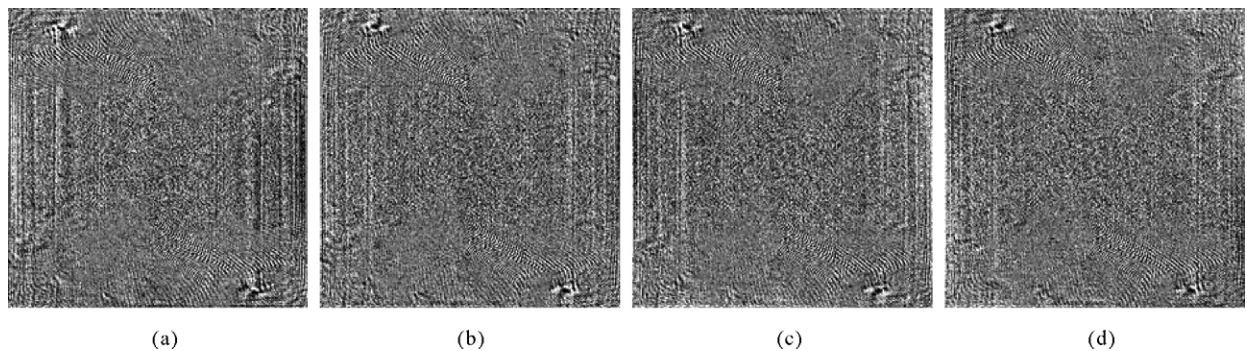


**Fig. 4.** The fast quaternion Fourier transform results of 24-bit color image Barbara: (a) the real part A, (b) the imaginary part C, (c) the imaginary part D, and (d) the imaginary part E.

One defines the Lagrangian

$$L(\omega, b, e, \alpha) = \frac{1}{2} \omega^T \omega + C \sum_{i=1}^l e_i^2 - \sum \alpha_i [y_i (\omega^T \phi(x_i) + b) - 1 + e_i] \quad (11)$$

With Lagrangian multipliers  $\alpha_i \in \mathbb{R}$ . The conditions for optimality are given by

$$\begin{cases} \frac{\partial L}{\partial \omega} = 0 \rightarrow \omega = \sum_{i=1}^l \alpha_i y_i \phi(x_i) \\ \frac{\partial L}{\partial b} = 0 \rightarrow \sum_{i=1}^l \alpha_i y_i = 0 \\ \frac{\partial L}{\partial e_i} = 0 \rightarrow \alpha_i = Ce_i \quad i = 1, \dots, l \\ \frac{\partial L}{\partial \alpha_i} = 0 \rightarrow y_i [w^T \varphi(x_i) + b] - 1 + e_i = 0 \quad i = 1, \dots, l \end{cases} \quad (12)$$

By eliminating  $e, \omega$ , one obtains the KKT system

$$\begin{bmatrix} 0 & Y^T \\ Y & \mathcal{Q} + C^{-1}I \end{bmatrix} \begin{bmatrix} b \\ \alpha \end{bmatrix} = \begin{bmatrix} 0 \\ \bar{1} \end{bmatrix} \quad (13)$$

where  $C$  is a positive constant,  $b$  is the bias.

$$y = (y_1, \dots, y_l)^T, \quad \bar{1} = (1, \dots, 1), \quad \alpha = (\alpha_1, \dots, \alpha_l)$$

and

$$\mathcal{Q}_{ij} = y_i y_j \phi(x_i)^T \phi(x_j) = y_i y_j K(x_i, x_j) \quad (1 \leq i, j \leq l) \quad (14)$$

Because LS-SVM does not incorporate the support vector selection method, the resulting network size is usually much larger than the original SVM. To solve this problem, a pruning method can be used to achieve sparseness in LS-SVM (Vapnik, 1995). The pruning technique reduces the complexity of the network by eliminating as much hidden neurons as possible.

## 5. Watermark embedding scheme

In this paper, we propose a new image watermarking algorithm with good visual quality and reasonable resistance toward geometric distortions. Firstly, the original color image is divided into color image blocks. Then, the fast quaternion Fourier transform is performed on the color image blocks. Finally, the digital watermark is embedded into original color image by adaptively modulating the real quaternion Fourier transform coefficients of color image blocks.

Let

$$I = \{R(x, y), G(x, y), B(x, y)\} \quad (0 \leq x < M, 0 \leq y < N)$$

denote a host digital image (color image), and  $R(x, y), G(x, y), B(x, y)$  are the color component values at position  $(x, y)$ .

$W = \{w(i, j), 0 \leq i < P, 0 \leq j < Q\}$  is a binary image to be embedded within the host image, and  $w(i, j) \in \{0, 1\}$  is the pixel value at  $(i, j)$ . The digital watermark embedding scheme can be summarized as follows.

### Step 1: watermark preprocessing

In order to dispel the pixel space relationship of the binary watermark image, and improve the robustness of the whole digital watermark system, watermark scrambling algorithm is used at first. In our watermark embedding scheme, the binary watermark image is scrambled from  $W$  to  $W_1$  by using Arnold transform. Arnold transform is also called Cat Face transfer, and it is given by

$$\begin{pmatrix} x' \\ y' \end{pmatrix} = \begin{pmatrix} 1 & 1 \\ 1 & 2 \end{pmatrix} \begin{pmatrix} x \\ y \end{pmatrix} \pmod{N} \quad (15)$$

where  $(x, y)$  is the pixel of the watermark image,  $(x', y')$  is the pixel of the watermark image after scrambling,  $N$  is order of watermark image matrix. Since the Arnold transform is periodic, the number of scrambling can be considered as the key to enhance the security.

After that, the scrambled binary watermark  $W_1$  is divided into watermark blocks  $W_k$  of  $2 \times 2$  bits

$$W_k = \{w_k(i, j), 0 \leq i \leq 1, 0 \leq j \leq 1\} \quad (k = 1, 2, \dots, p/2 * Q/2) \quad (16)$$

### Step 2: original color image blocking

The original color image  $I$  is divided into small color image blocks  $B_k$  of  $8 \times 8$  pixels

$$B_k = \{b_k(i, j), 0 \leq i \leq 7, 0 \leq j \leq 7\} \quad (k = 1, 2, \dots, M/8 * N/8) \quad (17)$$

### Step 3: fast quaternion Fourier transform of color image block

The fast quaternion Fourier transform is performed on the color image block  $B_k$  ( $k = 1, 2, \dots, M/8 * N/8$ ), and a real coefficient matrix  $A_k$  and three imaginary coefficient matrices  $C_k, D_k, E_k$  are obtained (see Section 3.2).

### Step 4: digital watermark embedding

In our digital watermark embedding scheme, the block watermark embedding strategy is adopted. The watermark block  $W_k$  with  $2 \times 2$  watermark bits is embedded into the color image blocks  $B_k$  with  $8 \times 8$  pixels by modifying the real quaternion Fourier transform coefficients, as shown in Fig. 5.

$$\begin{aligned} a'_k(1, 1) &= \begin{cases} 2\Delta * \text{round}(a_k(1, 1)/2\Delta) + \Delta/2 & \text{if } w_k(0, 0) = 1 \\ 2\Delta * \text{round}(a_k(1, 1)/2\Delta) - \Delta/2 & \text{if } w_k(0, 0) = 0 \end{cases} \\ a'_k(1, 2) &= \begin{cases} 2\Delta * \text{round}(a_k(1, 2)/2\Delta) + \Delta/2 & \text{if } w_k(0, 1) = 1 \\ 2\Delta * \text{round}(a_k(1, 2)/2\Delta) - \Delta/2 & \text{if } w_k(0, 1) = 0 \end{cases} \\ a'_k(2, 1) &= \begin{cases} 2\Delta * \text{round}(a_k(2, 1)/2\Delta) & \text{if } w_k(1, 0) = 1 \\ 2\Delta * \text{round}(a_k(2, 1)/2\Delta) & \text{if } w_k(1, 0) = 0 \end{cases} \\ a'_k(2, 2) &= \begin{cases} 2\Delta * \text{round}(a_k(2, 2)/2\Delta) & \text{if } w_k(1, 1) = 1 \\ 2\Delta * \text{round}(a_k(2, 2)/2\Delta) & \text{if } w_k(1, 1) = 0 \end{cases} \end{aligned} \quad (18)$$

where  $W_k = \{w_k(i, j), 0 \leq i \leq 1, 0 \leq j \leq 1\}$  is the digital watermark block,  $A_k = \{a_k(i, j), 0 \leq i \leq 7, 0 \leq j \leq 7\}$  is the old real quaternion Fourier transform coefficients block of color image blocks  $B_k$ ,  $A'_k = \{a'_k(i, j), 0 \leq i \leq 7, 0 \leq j \leq 7\}$  is the new real quaternion Fourier transform coefficients block,  $\text{round}(\cdot)$  denotes round operator,  $\Delta$  is the watermark embedding strength.

### Step 5: symmetric quaternion Fourier transform coefficients modification

From the quaternion representation of color image, we know that the watermarked color image should also be represented in pure quaternion form after inverse quaternion Fourier transform so as to transmit high-quality watermarked image in RGB color

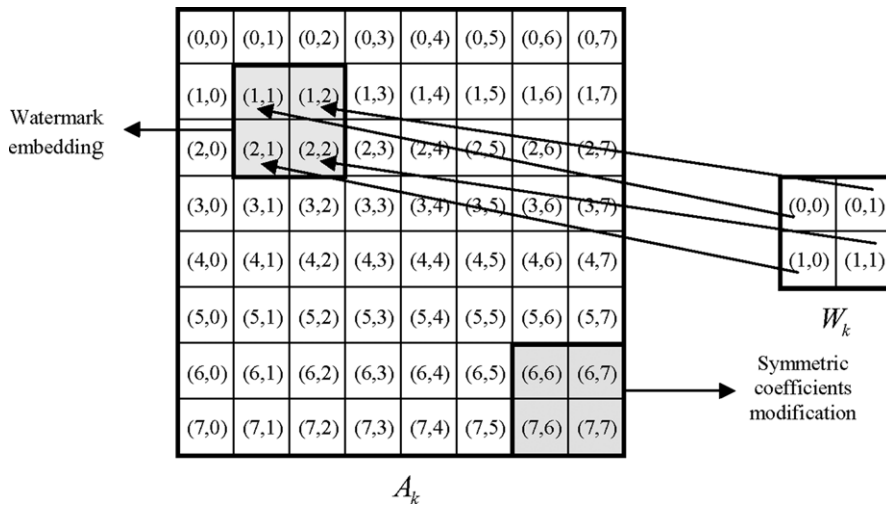


**Fig. 5.** The digital watermark embedding.

space (or other color space). In order to obtain the pure quaternion representation of watermarked color image, we must modify the symmetric real quaternion Fourier transform coefficients (Jiang et al., 2008) (see Fig. 5).

$$a'_k(6, 6) = -a'_k(2, 2)$$

$$a'_k(6, 7) = -a'_k(2, 1)$$

$$a'_k(7, 6) = -a'_k(1, 2)$$

$$a'_k(7, 7) = -a'_k(1, 1), \quad k = 1, 2, \dots, P/2 * Q/2 \quad (19)$$

where  $a'_k(i, j)$  is the new real coefficients of quaternion Fourier transform.

#### Step 6: obtaining the watermarked color image block

The watermarked color image block  $B'_k$  ( $k = 1, 2, \dots, P/2 * Q/2$ ) can be obtained by performing the inverse quaternion Fourier transform, in which the new real coefficient matrix is used instead of the old real coefficient matrix.

#### Step 7: obtaining the watermarked image

In order to improve furtherly the watermarking performance, we repeat the step 3-step 6 to embed  $(M * N/16 * P * Q) - 1$  copies of digital watermark into other color image blocks. Finally, the watermarked color image  $I'$  can be obtained by combining the watermarked color image blocks.

## 6. Watermark detection scheme

According to quaternion Fourier transform and pseudo-Zernike moments, a robust color image watermarking detection using LS-SVM correction is proposed, and it can be summarized as follows: (1) Fast quaternion Fourier transform is performed on the training images, which produce a real coefficient matrix and three imaginary coefficient matrices, (2) Some low-order pseudo-Zernike moments of the real coefficient matrix are computed, which are regarded as the effective feature vectors, (3) The appropriate kernel function is selected for training, and a LS-SVM training model can be obtained, (4) The watermarked color image is corrected with the well trained LS-SVM model, (5) The digital watermark is extracted from the corrected watermarked color image.

Let

$$I^* = \{R(x, y)^*, G(x, y)^*, B(x, y)^*\} \quad (0 \leq x < M^*, 0 \leq y < N^*)$$

denote the watermarked color image, and  $R(x, y)^*$ ,  $G(x, y)^*$ ,  $B(x, y)^*$  are the color component values at position  $(x, y)$ . The main steps of the watermark detecting procedure developed can be described as follows.

### 6.1. Constructing the training images

Generally speaking, geometric distortions include various forms, such as rotation, scaling, translation, and cropping. Here, we only discuss the familiar geometric distortions including rotation, scaling, and translation. In order to obtain the LS-SVM training model, we must construct the training images  $H^k$  ( $k = 0, 1, \dots, K - 1$ ). In fact, the training images can be constructed by moving (including X-axis and Y-axis), rotating, and scaling an arbitrary color image. In this paper, we construct the training image samples by moving, rotating and scaling the watermarked color image.

### 6.2. LS-SVM training

Firstly, the fast quaternion Fourier transform is performed on the training image  $H^k$  ( $k = 0, 1, \dots, K - 1$ ), which produces a real coefficient matrix  $A^k$  ( $k = 0, 1, \dots, K - 1$ ) and three imaginary coefficient matrices  $C^k, D^k, E^k$  ( $k = 0, 1, \dots, K - 1$ ).

Secondly, 6 low-order pseudo-Zernike moments  $(f_1^k, f_2^k, f_3^k, f_4^k, f_5^k, f_6^k)$  ( $k = 0, 1, \dots, K - 1$ ) of the real coefficient matrix  $A^k$  are computed, which are regarded as image features for training. The pseudo-Zernike moments are robust image feature descriptors. It has been proven that the set of pseudo-Zernike moments can provide a compact, fixed-length and computation effective representation of the image content, and only a small fixed number of compact pseudo-Zernike moments need to be stored to effectively characterize the image content. Considering that we will discuss global geometric distortions, we select 6 low-order pseudo-Zernike moments  $|M_{00}|, |M_{01}|, |M_{10}|, |M_{11}|, |M_{02}|, |M_{20}|$  (we denote them as  $f_1, f_2, f_3, f_4, f_5, f_6$ , respectively) to reflect the global information of digital image (Khotanzad and Hong, 1990).

Thirdly, the corresponding geometrical attack (X-translation, Y-translation, scaling, and rotation) parameters  $t_x^k, t_y^k, s^k, \theta^k$  ( $k =$



**Fig. 6.** The geometric correction results for watermarked color image Barbara: (a) the watermarked color image with rotation 45°, (b) the corrected watermarked color image with rotation 45°, (c) the watermarked color image with translation (H 0,V 30), (d) the corrected watermarked color image with translation (H 0,V 30), (e) the watermarked color image with scaling (1.2), and (f) the corrected watermarked color image with scaling (1.2). (For interpretation of the references to color in this figure legend, the reader is referred to the web version of the article.)

$0, 1, \dots, K - 1$ ) are described as the training objective (see Section 6.1). Here,  $t_x, t_y, s, \theta$  represent X-direction moving distance, Y-direction moving distance, scaling factor, and rotation angle, respectively.

Then, we can obtain the training samples as following

$$\Omega_k = (f_1^k, f_2^k, f_3^k, f_4^k, f_5^k, f_6^k, t_x^k, t_y^k, s^k, \theta^k) \quad (k = 0, 1, \dots, K - 1)$$

For the linear transformation like rotation, scaling, and translation, there is no coupling among the 4 outputs, so we adopt the MIMO system constructed by 4 LS-SVM parallel structures

which is with 4 inputs, and the LS-SVM model can be obtained by training.

### 6.3. Geometric correction of watermarked color image

In order to extract accurately digital watermark, we firstly use LS-SVM training model to predict the data of watermarked color image, and then correct the watermarked color image according to the predicted value for resisting the geometric distortions. The

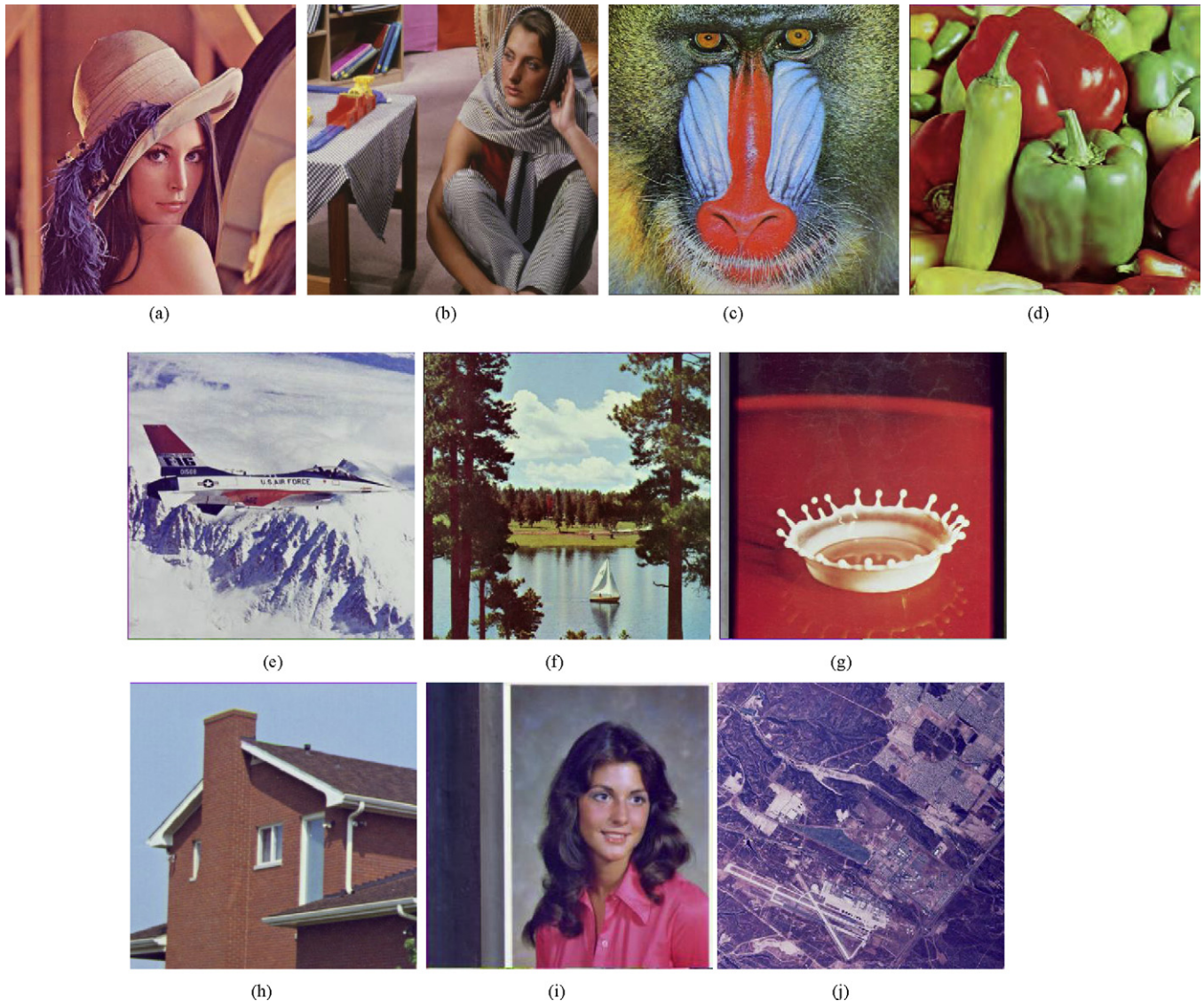


**Fig. 7.** The host color images used in experiment: (a) Lena, (b) Barbara, (c) Mandrill, (d) peppers, (e) airplane, (f) sailboat and lake, (g) splash, (h) house, (i) girl, and (j) San Diego. (For interpretation of the references to color in this figure legend, the reader is referred to the web version of the article.)

process of correcting watermarked image based on LS-SVM is as follows.

- (1) Perform fast quaternion Fourier transform on the watermarked color image  $I^*$ , which produces a real coefficient matrix  $A^*$  and three imaginary coefficient matrices  $C^*, D^*, E^*$ .
- (2) Compute 6 low-order pseudo-Zernike moments of the real coefficient matrix  $A^*(|M_{00}^*|, |M_{01}^*|, |M_{10}^*|, |M_{11}^*|, |M_{02}^*|, |M_{20}^*|)$  and let them be the input vectors.
- (3) The actual output  $t_x^*, t_y^*, s^*, \theta^*$  (geometric transformation parameters) is predicted by using the well trained LS-SVM model.
- (4) Correct the geometric distortions of watermarked color image  $I^*$  (that is inverse transformation such as rotation angle, and translation parameters) by using the obtained geometric transformation parameters  $t_x^*, t_y^*, s^*, \theta^*$  so that we can get the corrected watermarked image  $\hat{I}$ .

**Fig. 6** shows the geometric correction results for standard image Barbara.

#### 6.4. Watermark extraction

The watermark extraction procedure in the proposed scheme neither needs the original color image nor any other side information. Let  $\hat{I}$  denote the corrected watermarked color image, the main steps of watermark extraction can be described as follows.

**Step 1:** The corrected watermarked color image  $\hat{I}$  is divided into small color image blocks  $\hat{B}_k$  of  $8 \times 8$  pixels

$$\hat{B}_k = \{\hat{b}_k(i, j), 0 \leq i \leq 7, 0 \leq j \leq 7\} \quad (k = 1, 2, \dots, \hat{M}/8 * \hat{N}/8)$$

**Step 2:** The fast quaternion Fourier transform is performed on the watermarked color image block  $\hat{B}_k$  ( $k = 1, 2, \dots, \hat{M}/8 * \hat{N}/8$ ), and a real coefficient matrix  $\hat{A}_k$  and three imaginary coefficient matrices  $\hat{C}_k, \hat{D}_k, \hat{E}_k$  are obtained (see Section 2.2).

**Step 3:** The watermark block  $\hat{W}_k$  ( $k = 1, 2, \dots, P/2 * Q/2$ ) with  $2 \times 2$  watermark bits are extracted from the real coefficient matrix  $\hat{A}_k$  of the watermarked color image blocks  $\hat{B}_k$  as follows:

$$\hat{w}_k(0, 0) = \begin{cases} 1 & \text{if } \hat{a}_k(1, 1) - 2\Delta * \text{round}(\hat{a}_k(1, 1)/2\Delta) > 0 \\ 0 & \text{if } \hat{a}_k(1, 1) - 2\Delta * \text{round}(\hat{a}_k(1, 1)/2\Delta) \leq 0 \end{cases}$$

$$\hat{w}_k(0, 1) = \begin{cases} 1 & \text{if } \hat{a}_k(1, 2) - 2\Delta * \text{round}(\hat{a}_k(1, 2)/2\Delta) > 0 \\ 0 & \text{if } \hat{a}_k(1, 2) - 2\Delta * \text{round}(\hat{a}_k(1, 2)/2\Delta) \leq 0 \end{cases}$$

$$\hat{w}_k(1, 0) = \begin{cases} 1 & \text{if } \hat{a}_k(2, 1) - 2\Delta * \text{round}(\hat{a}_k(2, 1)/2\Delta) > 0 \\ 0 & \text{if } \hat{a}_k(2, 1) - 2\Delta * \text{round}(\hat{a}_k(2, 1)/2\Delta) \leq 0 \end{cases}$$

$$\hat{w}_k(1, 1) = \begin{cases} 1 & \text{if } \hat{a}_k(2, 2) - 2\Delta * \text{round}(\hat{a}_k(2, 2)/2\Delta) > 0 \\ 0 & \text{if } \hat{a}_k(2, 2) - 2\Delta * \text{round}(\hat{a}_k(2, 2)/2\Delta) \leq 0 \end{cases}$$

$$(k = 1, 2, \dots, P/2 * Q/2) \quad (20)$$

where  $\hat{W}_k = \{\hat{w}_k(i, j), 0 \leq i \leq 1, 0 \leq j \leq 1\}$  is the extracted digital watermark block,  $\hat{A}_k = \{\hat{a}_k(i, j)\}$  is the real quaternion Fourier transform coefficients matrix of watermarked color image blocks,  $\text{round}(\cdot)$  denotes round operator,  $\Delta$  is the watermark embedding strength.

**Table 1**  
The average performance of the proposed watermarking method.

Watermark	Average PSNR (no attack)	Average BER						
		Median filtering (3 × 3)	Salt and peppers noise (0.01)	JPEG 50	Histogram equalization	Light increasing	Rotation15°	Scaling 1.5
A	40.24 dB	0.0134	0.0146	0.0283	0.0103	0.0162	0.0214	0.0206
B	39.92 dB	0.0140	0.0139	0.0290	0.0116	0.0175	0.0221	0.0210
C	40.31 dB	0.0148	0.0148	0.0282	0.0123	0.0163	0.0233	0.0204
D	40.07 dB	0.0137	0.0153	0.0281	0.0106	0.0166	0.0242	0.0202
E	39.54 dB	0.0151	0.0151	0.0294	0.0108	0.0172	0.0205	0.0216
F	41.01 dB	0.0139	0.0157	0.0296	0.0111	0.0180	0.0209	0.0227
G	39.89 dB	0.0145	0.0145	0.0293	0.0118	0.0158	0.0220	0.0215
H	40.34 dB	0.0148	0.0147	0.0288	0.0126	0.0159	0.0217	0.0203
I	40.06 dB	0.0150	0.0148	0.0282	0.0130	0.0167	0.0218	0.0212

**Table 2**  
The low-order pseudo-Zernike moments under different common image processing operations.

Test image	Low-order pseudo-Zernike moments					
	M <sub>00</sub>	M <sub>01</sub>	M <sub>10</sub>	M <sub>11</sub>	M <sub>02</sub>	M <sub>20</sub>
Origin image	12,500	12,876	6847	6223	7631	7317
Image under median filtering (3 × 3)	12,534	12,884	6867	6232	7646	7323
Image under Gaussian noise (0.05)	12,542	12,885	6853	6234	7640	7328
Image under JPEG 70 compression	12,488	12,863	6830	6209	7613	7303
Image under edge sharpening	12,527	12,934	6886	6253	7685	7360

**Table 3**  
The SVM prediction performance for training image and test image.

Image	Geometric transformation parameters							
	Rotation	Rotation	Scaling	Scaling	X-translation	X-translation	Y-translation	Y-translation
<b>Training image</b>								
Actual distortion parameters	7.2°	10°	0.86	0.9	8	10	8	10
Predicted distortion parameters	7.200°	10.003°	0.860	0.902	8.000	9.999	8.000	10.002
<b>Test image</b>								
Actual distortion parameters	7.2°	10°	0.86	0.9	8	10	8	10
Predicted distortion parameters	7.201°	10.004°	0.859	0.903	8.002	10.004	8.001	10.003

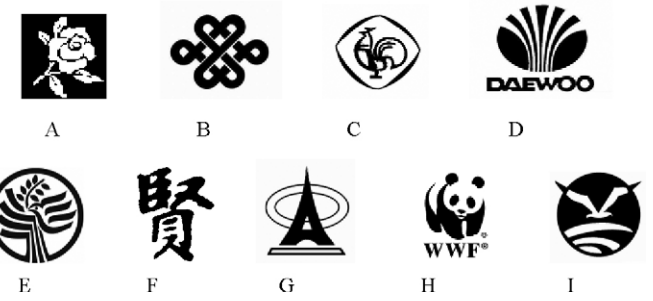


**Fig. 8.** Digital watermarks A through I used in experiments.

#### Step 4: The digital watermark

$$\hat{W} = \{\hat{w}(i, j), 0 \leq i < P, 0 \leq j < Q\}$$

can be obtained by the watermark block combination and inverse scrambling operation.

Finally, the optimal digital watermark  $W^* = \{w^*(i, j), 0 \leq i < P, 0 \leq j < Q\}$  can be obtained according to the majority rule.

#### 7. Simulation results

We test the proposed watermarking scheme on ten popular test images and nine test digital watermarks. Ten test images

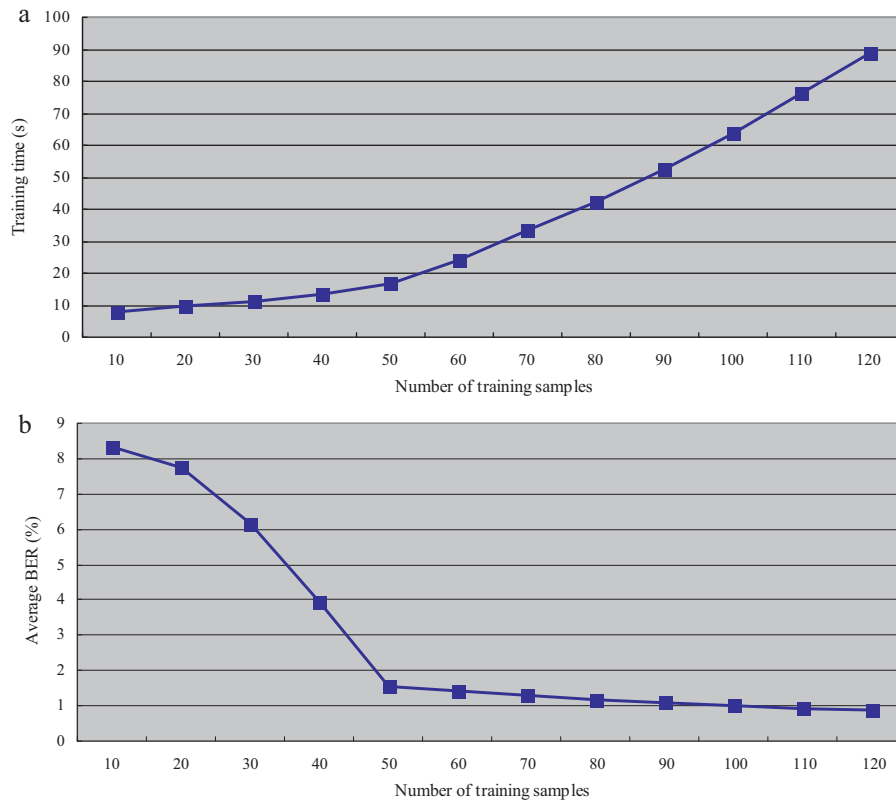


**Fig. 9.** The relationship between training time, average BER, and number of training samples: (a) the relationship between training time and the number of training samples and (b) the relationship between average BER and the number of training samples.

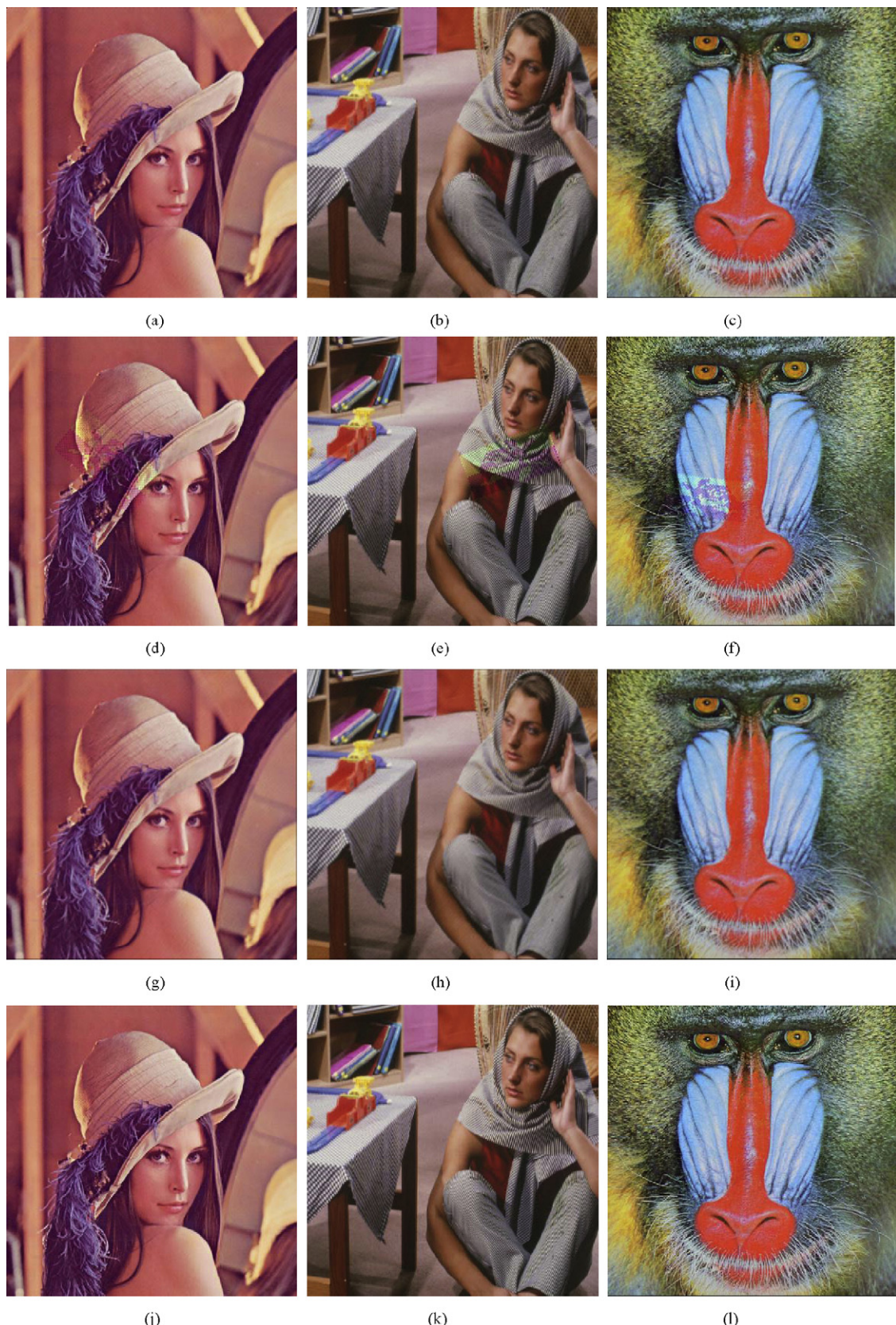
from USC-SIPI image database (Kumar and Santhi, 2011), each of dimensions  $256 \times 256 \times 24$ bit, are shown in Fig. 7, referred to as “Lena”, “Barbara”, “Mandrill”, “Peppers”, “Airplane”, “Sailboat and lake”, “Splash”, “House”, “Girl”, and “San Diego”, respectively, in the sequel. And nine test watermarks, each of dimensions  $64 \times 64$ , are shown in Fig. 8, hereinafter referred to as watermarks A, B, C, D, E, F, G, H, and I, respectively. The number of training samples is  $K = 50$ , the watermark embedding strength is  $\Delta = 270$ , and the radius-based function (RBF) is selected as the LS-SVM kernel function. Also, the experimental results are compared with schemes in

**Table 5**  
The PSNR and time results for various watermarking methods.

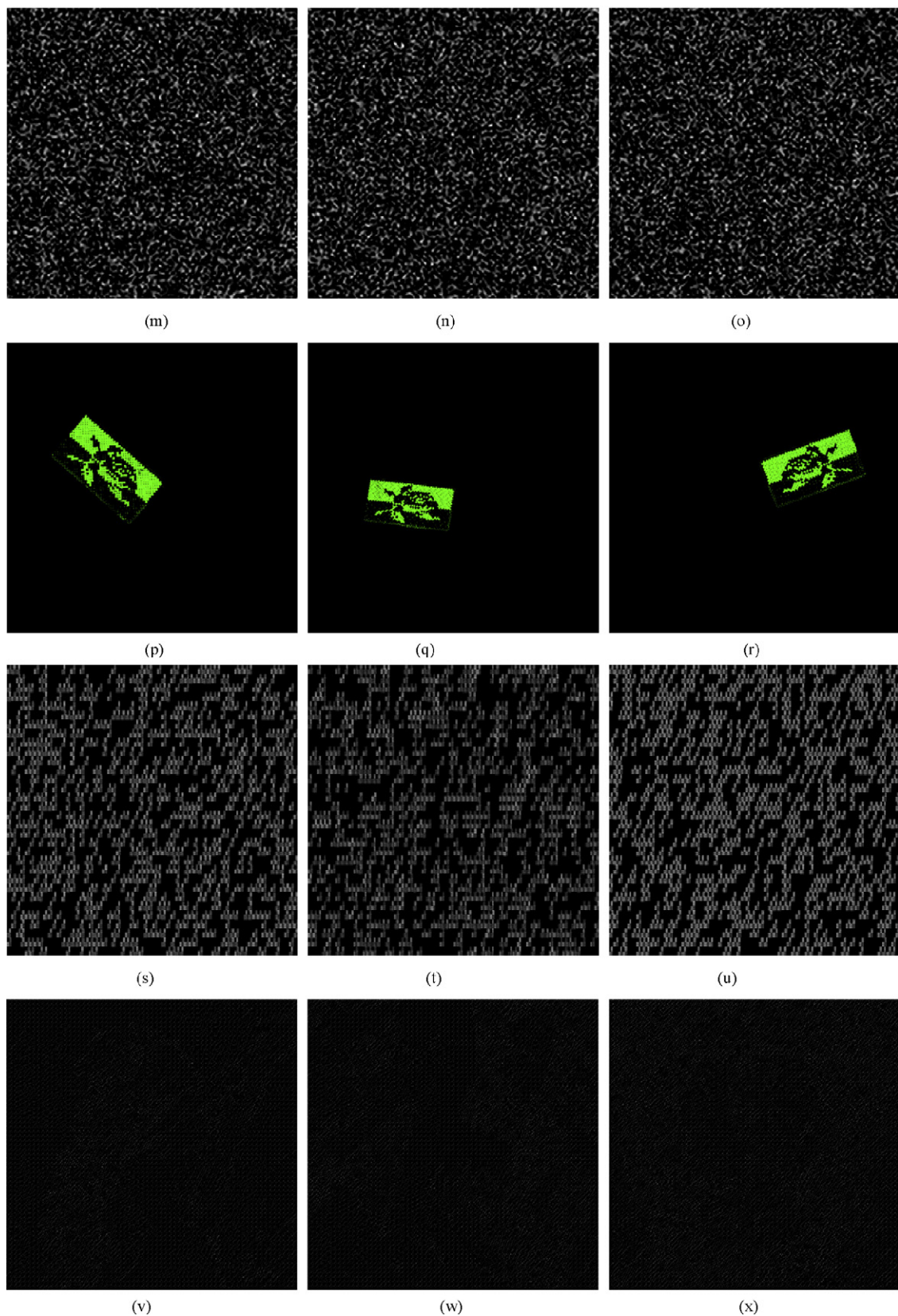
Method	PSNR (dB)		
	Lena	Barbara	Mandrill
Scheme in Chou and Liu (2010)	39.92	39.98	39.45
Scheme in Niu et al. (2011)	40.57	40.71	41.76
Scheme in Tsui et al. (2008)	33.21	33.15	32.62
Proposed scheme	36.10	35.55	34.43

**Table 4**  
The BER values before and after using LS-SVM classification.

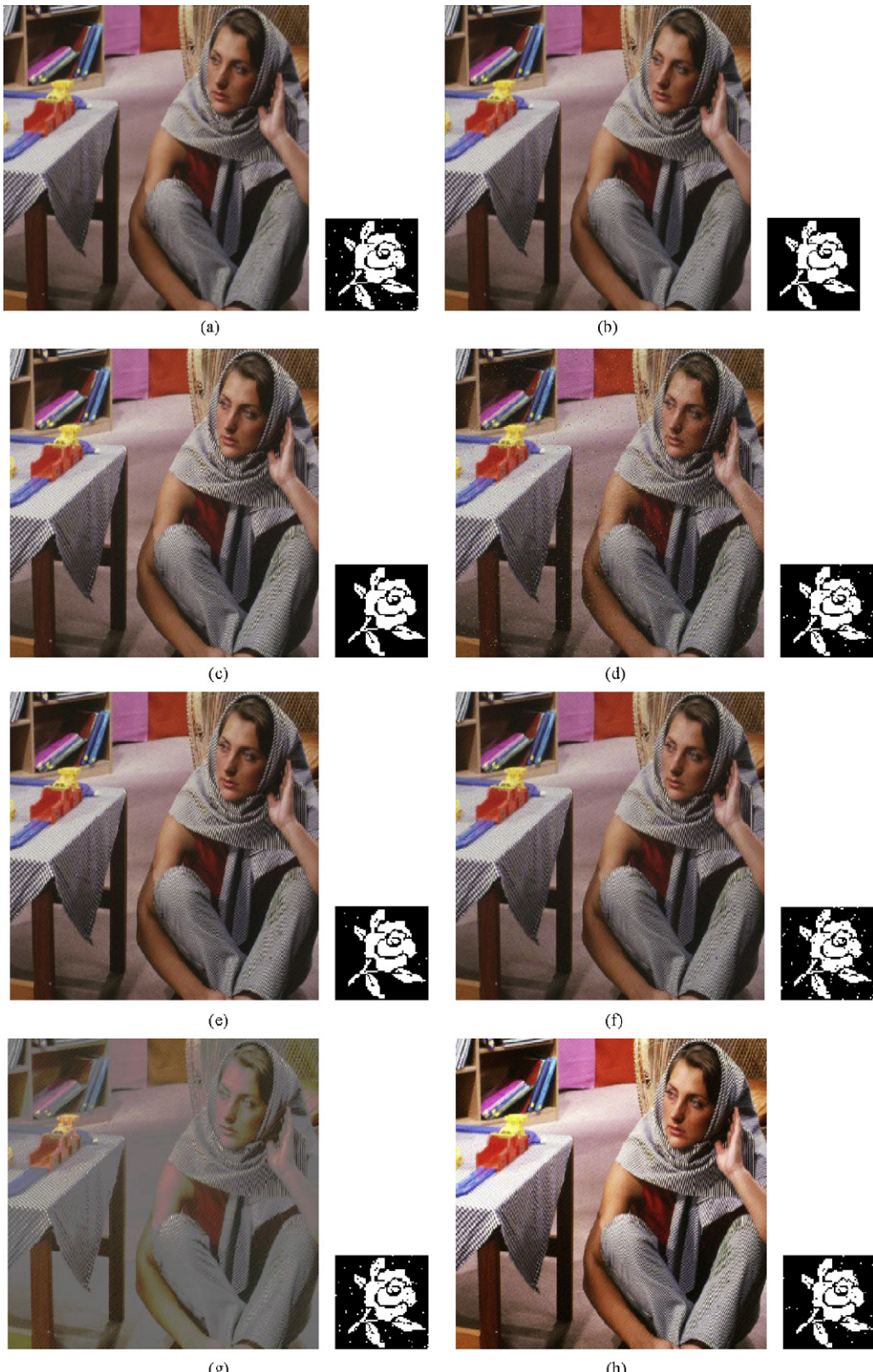
Attacks	Lena		Barbara		Mandrill	
	After using LS-SVM classification	Before using LS-SVM classification	After using LS-SVM classification	Before using LS-SVM classification	After using LS-SVM classification	Before using LS-SVM classification
Median filtering ( $3 \times 3$ )	0.0100	0.0100	0.0493	0.0493	0.1531	0.1531
Gaussian filtering ( $3 \times 3$ )	0	0	0.0034	0.0034	0.0098	0.0098
Average filtering ( $3 \times 3$ )	0.0237	0.0237	0.0549	0.0549	0.1531	0.1531
Gaussian noise (0.05)	0.0522	0.0522	0.0620	0.0620	0.0564	0.0564
Salt and peppers noise (0.01)	0.0154	0.0154	0.0134	0.0134	0.0134	0.0134
JPEG	70	0.0004	0.0004	0.0015	0.0015	0.0095
	50	0.0208	0.0208	0.0300	0.0300	0.0491
Rotation	5°	0.0029	N/A	0.0142	N/A	0.0557
	15°	0.0088	N/A	0.0217	N/A	0.0857
Scaling	0.5	0.0745	N/A	0.1211	N/A	0.2427
	1.2	0.0046	N/A	0.0225	N/A	0.0930
Translation	(H 2,V 15)	0	N/A	0	N/A	0
	(H 15,V 2)	0	N/A	0	N/A	0
Cropping	Centered cropping	0	0	0	0	0
	10% off					
	Centered cropping	0	0	0	0	0
	20% off					
Length-width ratio change	(0.8,1.0)	0	N/A	0.0017	N/A	0.0464
	(1.0,0.8)	0.0015	N/A	0.0085	N/A	0.0342



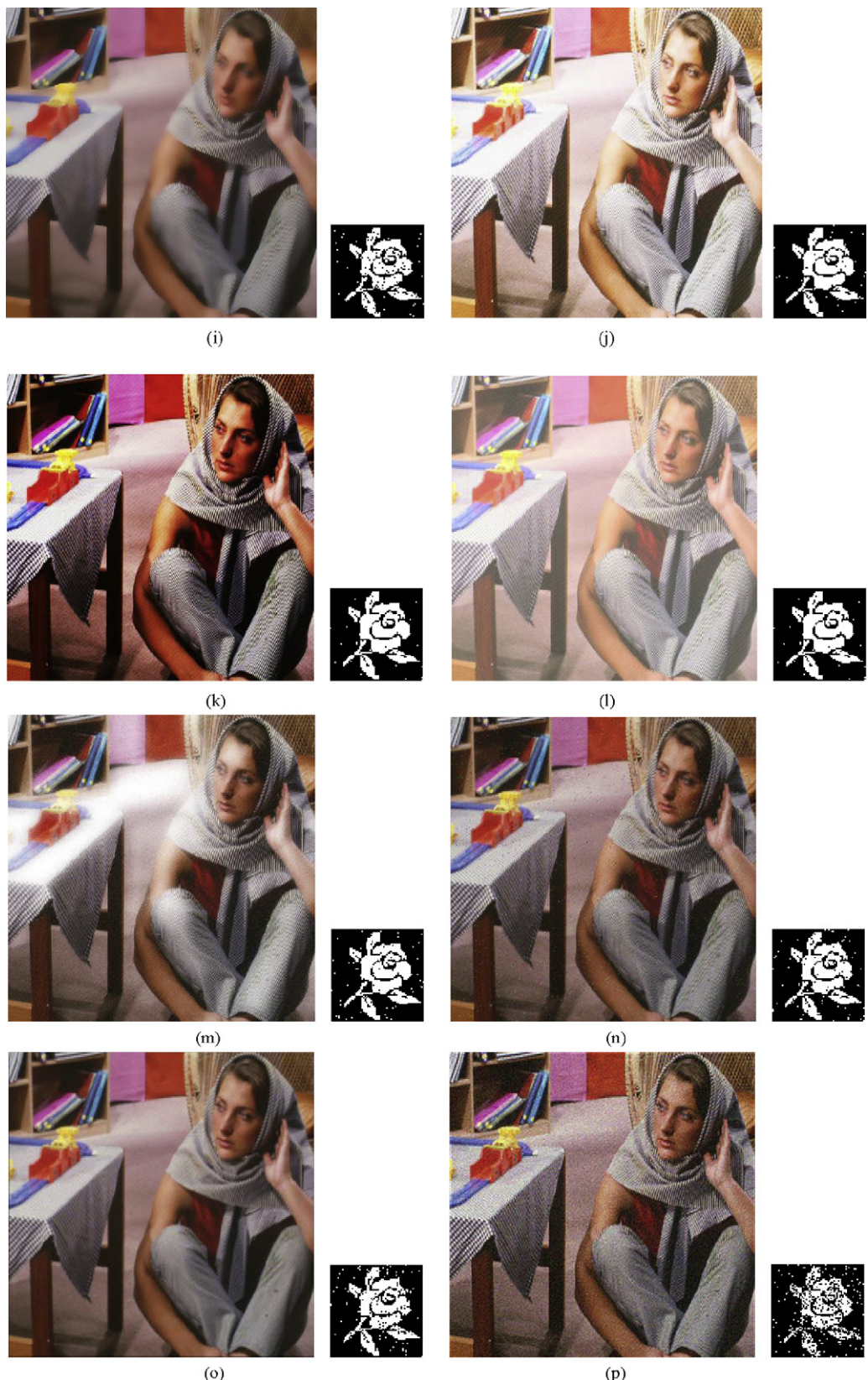
**Fig. 10.** The watermark embedding examples by using our algorithm, scheme (Chou and Liu, 2010), scheme (Niu et al., 2011), and scheme (Tsui et al., 2008): (a)–(c) the watermarked image using scheme (Chou and Liu, 2010), (d)–(f) the watermarked image using scheme (Niu et al., 2011), (g)–(i) the watermarked image using scheme (Tsui et al., 2008), (j)–(l) the watermarked image using our algorithm, (m)–(o) the absolute difference between origin image and watermarked image for scheme (Chou and Liu, 2010), (p)–(r) the absolute difference between origin image and watermarked image for scheme (Niu et al., 2011), (s)–(u) the absolute difference between origin image and watermarked image for scheme (Tsui et al., 2008), and (v)–(x) the absolute difference between origin image and watermarked image for our algorithm.



**Fig. 10.** (Continued).



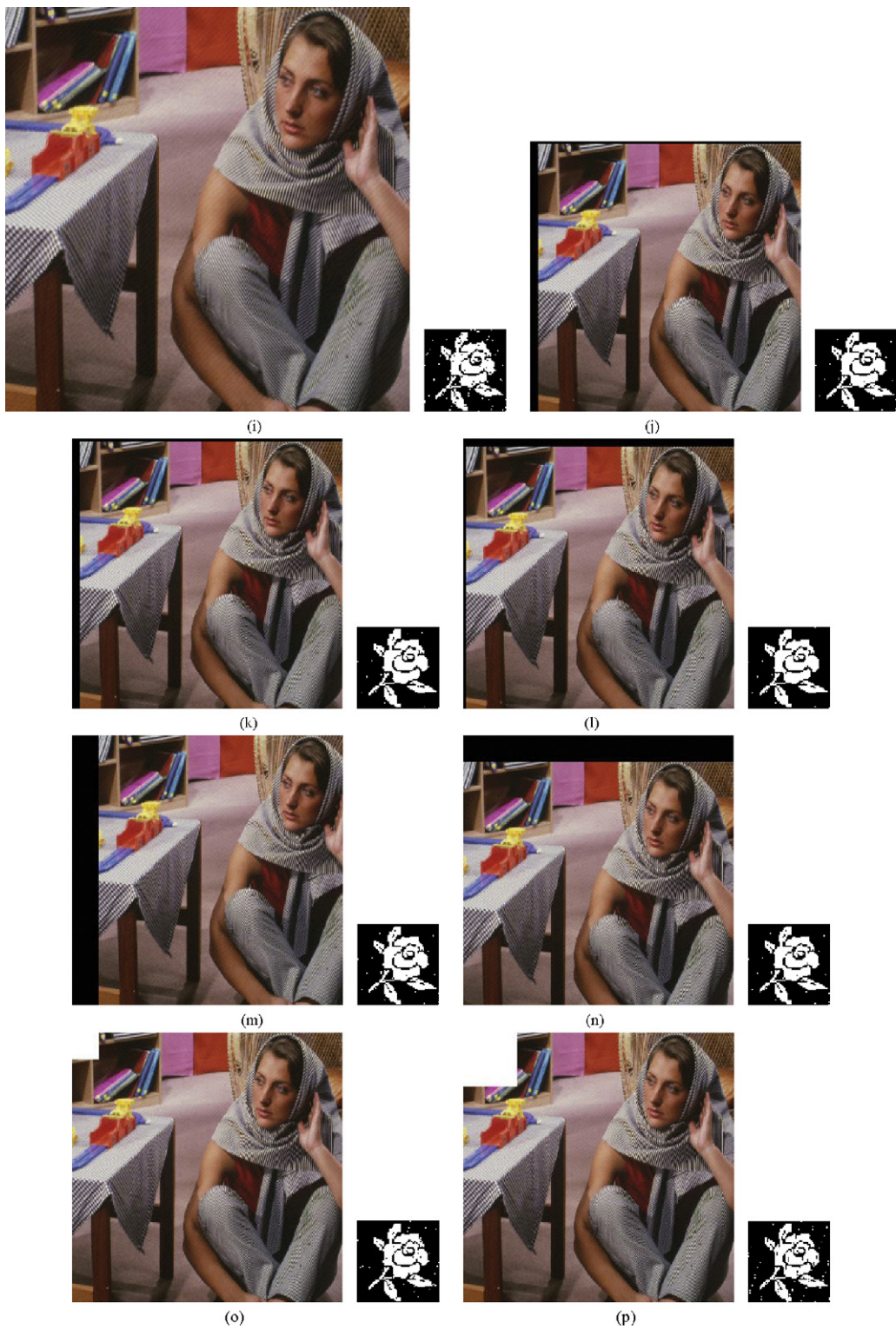
**Fig. 11.** The attacked (common image processing operations) watermarked image and the extracted watermark: (a) median filtering ( $3 \times 3$ ), BER = 0.0193, (b) Gaussian filter ( $3 \times 3$ ), BER = 0.0034, (c) random noise (10), BER = 0, (d) salt and peppers noise (0.01), BER = 0.0134, (e) JPEG 70, BER = 0.0015, (f) JPEG 50, BER = 0.0213, (g) equalization, BER = 0.0205, (h) histogram equalization, BER = 0.0105, (i) image blurring (6,40), BER = 0.0276, (j) light increasing (100), BER = 0.0112, (k) contrast increasing (150), BER = 0.0076, (l) gamma correction, BER = 0.0076, (m) diffuse glow (4,8,16), BER = 0.0166, (n) salt and peppers noise (0.01)+ Gaussian filter ( $3 \times 3$ ), BER = 0.0203, (o) average filtering ( $3 \times 3$ ) + JPEG 70, BER = 0.0351, and (p) Gaussian noise (0.005)+ average filter ( $3 \times 3$ ) + edge sharpening, BER = 0.0990.



**Fig. 11.** (Continued).



**Fig. 12.** The attacked (geometric distortions) watermarked image and the extracted watermark: (a) rotation ( $5^\circ$ ), BER = 0.0142, (b) rotation ( $15^\circ$ ), BER = 0.0217, (c) rotation ( $45^\circ$ ), BER = 0.0273, (d) rotation ( $75^\circ$ ), BER = 0.0220, (e) rotation ( $90^\circ$ ), BER = 0.0032, (f) scaling (0.5), BER = 0.0533, (g) scaling (0.9), BER = 0.0273, (h) scaling (1.2), BER = 0.0225, (i) scaling (1.5), BER = 0.0222, (j) translation (H5,V15), BER = 0.0041, (k) translation (H20,V20), BER = 0.0047, (l) translation (H15,V5), BER = 0.0038, (m) translation (H0,V50), BER = 0.0046, (n) translation (H50,V0), BER = 0.0048, (o) cropping (10%), BER = 0.0091, (p) cropping (20%), BER = 0.0261, (q) cropping (50%), BER = 0.0753, (r) cropping (60%), BER = 0.0932, (s) length-width ratio change (0.8,1.0), BER = 0.0017, (t) length-width ratio change (1.2,1.0), BER = 0.0059, (u) length-width ratio change (1.0,0.8), BER = 0.0085, (v) rotation ( $5^\circ$ ) + scaling (0.9), BER = 0.0290, (w) rotation ( $15^\circ$ ) + translation (H5,V15), BER = 0.0352, (x) scaling (1.2) + Gaussian noise (0.05), BER = 0.0589, (y) JPEG 70 + scaling (0.9), BER = 0.0312, and (z) translation (H20,V20) + Gaussian filtering (3  $\times$  3), BER = 0.0046.

**Fig. 12.** (Continued).

(Niu et al., 2011; Tsui et al., 2008; Chou and Liu, 2010). The statistical results show that the average accurate rate of our image registration and Bartoli's image registration (Cheddad et al., 2010) are 94.2% and 95.3%, respectively.

Each of the nine test watermarks was embedded in the ten test images using the proposed watermarking method. A total of  $9 \times 10 = 90$  watermarked images were generated and for each

watermarked image, the digital was extracted under various attacks. Table 1 gives the average values of the PSNRs obtained after embedding a particular watermark in the ten test images, as well as the average values of the BER obtained under various attacks.

Table 2 gives the low-order pseudo-Zernike moments under different common image processing operations. Table 3 gives the LS-SVM prediction performance for training image and test image.

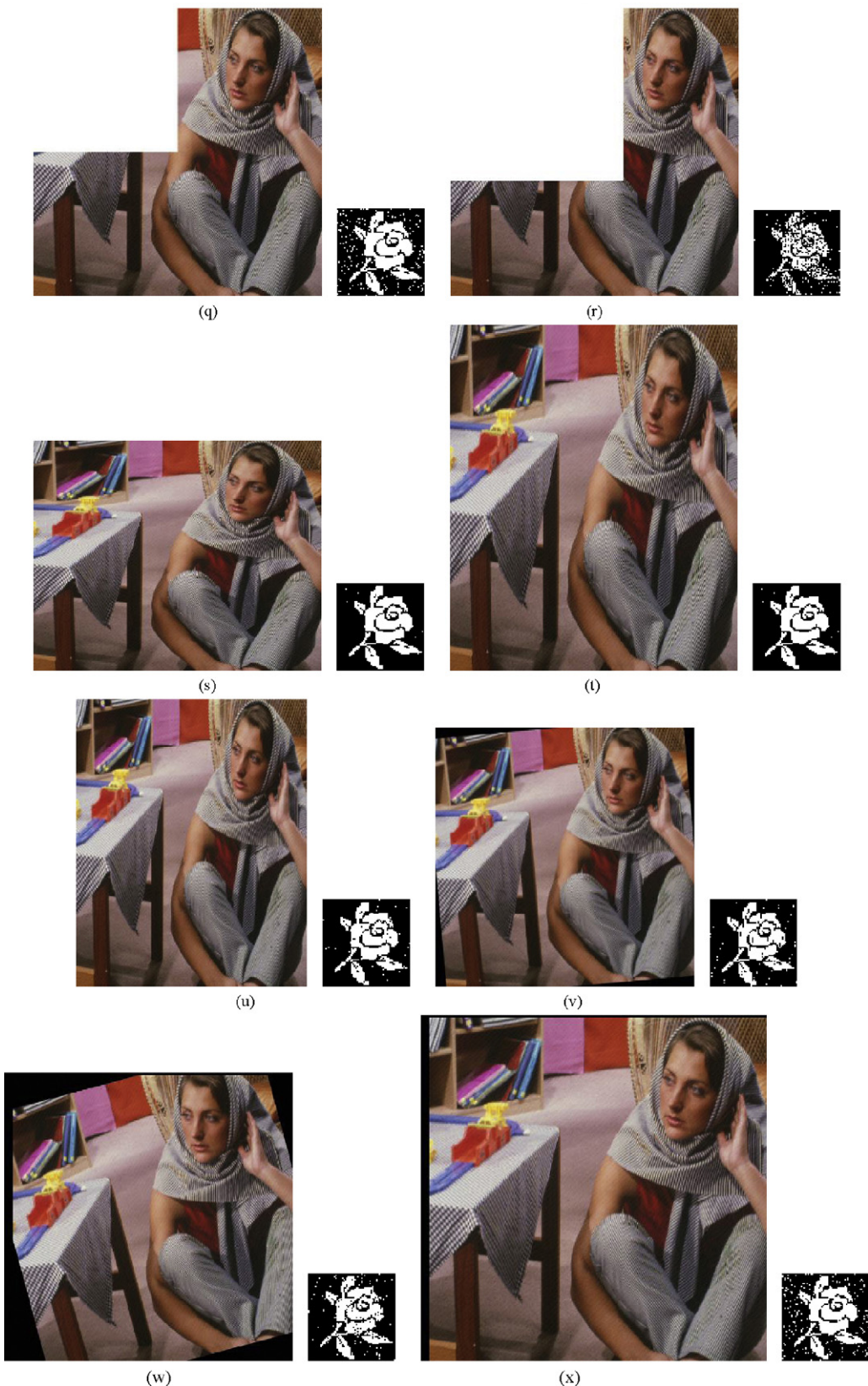


**Fig. 12.** (Continued).



Fig. 12. (Continued).

Fig. 9 shows the relationship between training time, average BER, and the number of training samples. Here, the average BER is obtained for 10 host images, 9 watermarks, and above 8 kinds of attacks. From the Fig. 9, we can see that the optimal number of training samples is  $K=50$ . Table 4 gives the comparison results of the BER values before and after using LS-SVM classification.

### 7.1. The quality of watermarked images

In this work, we use peak signal-to-noise ratio (PSNR) to measure the quality of watermarked images. It is defined as

$$\text{PSNR}(I, I^*) = 10 \log \left( \frac{255^2 \times M \times N}{\sum_{x=0}^{M-1} \sum_{y=0}^{N-1} [f(x, y) - f^*(x, y)]^2} \right)$$

where  $I$  is the original image and  $I^*$  is the watermarked version,  $M \times N$  is the size of digital image.

Fig. 10 is the result of applying our algorithm, scheme (Chou and Liu, 2010), scheme (Niu et al., 2011), and scheme (Tsui et al., 2008) for data embedding in a color image. Fig. 10(a)–(l) shows the watermarked image Lena, Barbara, and Mandrill using scheme (Chou and Liu, 2010), scheme (Niu et al., 2011), scheme (Tsui et al., 2008), and our algorithm. Fig. 10(m)–(x) is the absolute difference between origin image and watermarked image for scheme (Chou and Liu, 2010), scheme (Niu et al., 2011), scheme (Tsui et al., 2008), and our algorithm respectively, multiplied by 40 for better display. Table 5 gives the PSNR of different watermarking schemes.

### 7.2. Robustness to various attacks

Simulation results, which are obtained by the proposed watermarking scheme, for common image processing operations and geometric distortions are shown in Figs. 11 and 12 respectively. Tables 6 and 7 show the results of comparison with schemes (Niu et al., 2011; Tsui et al., 2008; Chou and Liu, 2010). In this study, reliability was measured as the bit error rate (BER) of extracted watermark, its definition is

$$\text{BER} = \frac{B}{P \times Q} \times 100\%$$

where  $B$  is the number of erroneously detected bits,  $P \times Q$  is the watermark image dimensions.

It is clear that the proposed scheme outperforms scheme (Niu et al., 2011; Tsui et al., 2008; Chou and Liu, 2010) under most attacks in terms of BER.

From the above measurements, several observations can be made.

- The proposed color image watermarking approach: This scheme provides satisfactory results for most attacks, especially for color attacks and geometric distortions. However, it is not very robust against some attacks, such as median filtering, light lowering, and length-width ratio change, for texture image such Mandrill. The underlying reason is that the proposed algorithm only modifies the real quaternion Fourier transform coefficients, but some attacks such as median filtering, light lowering, and length-width ratio change, can destroy significantly the real quaternion Fourier transform coefficients of texture image. Even though it cannot completely recover the embedded messages for these attacks, the BER is significantly smaller than the other three watermarking approaches. Another small disadvantage of it is that the computational complexity is slightly high for LS-SVM training and pseudo-Zernike moments computation.
- The perceptually tuned color image watermarking (Chou and Liu, 2010): The approach has good imperceptibility, because it is perceptually optimized by embedding high-strength watermark signals in wavelet coefficients of high perceptual redundancy. The strength of the embedded watermark signal is determined by the amount of perceptual redundancy inherent in the corresponding wavelet coefficient. However, it is fragile to some color attacks and geometric distortions, including gamma correction, rotation, translation, and length-width ratio change. The underlying reason is that it ignores the color channel correlation and the watermark desynchronization.
- The NSCT domain color image watermarking scheme (Niu et al., 2011): It provides good watermark imperceptibility, and satisfactory robustness to most attacks. But, it is not robust to some color attacks, such as histogram equalization, light increasing, contrast lowering, mosaic, and gamma correction. The underlying reason is that it only embeds the digital watermark into the image luminance component, and ignores the correlation between different color channels. Another disadvantage of it is that this algorithm

**Table 6**

The watermark detection results for common image processing operations (BER).

Attacks	Lena				Barbara				Mandrill			
	Proposed scheme	Scheme in Chou and Liu (2010)	Scheme in Niu et al. (2011)	Scheme in Tsui et al. (2008)	Proposed scheme	Scheme in Chou and Liu (2010)	Scheme in Niu et al. (2011)	Scheme in Tsui et al. (2008)	Proposed scheme	Scheme in Chou and Liu (2010)	Scheme in Niu et al. (2011)	Scheme in Tsui et al. (2008)
No attack	0	0.0098	0.0166	0	0	0.0107	0.0176	0.0042	0	0.0146	0.0020	0.0059
Median filtering (3 × 3)	0.0100	0.0514	0.0264	0.0676	0.0493	0.1083	0.0304	0.0677	0.1531	0.1121	0.032	0.0689
Gaussian filtering (3 × 3)	0	0.0432	0.0313	0.0781	0.0034	0.0451	0.0225	0.0705	0.0098	0.0501	0.0107	0.0801
Average filtering (3 × 3)	0.0237	0.0477	0.0303	0.0596	0.0549	0.0783	0.0234	0.0659	0.1531	0.0801	0.0049	0.0567
Gaussian noise (0.05)	0.0522	0.2122	0.0273	0.0622	0.0620	0.2217	0.0215	0.0612	0.0564	0.2416	0.0234	0.0646
Salt and peppers noise (0.01)	0.0154	0.0758	0.0234	0.0726	0.0134	0.0773	0.0164	0.0728	0.0134	0.0783	0.0205	0.0804
Random Noise (10)	0	0.0818	0.0293	0.0773	0	0.0879	0.0195	0.0684	0	0.0902	0.0059	0.0735
Edge Sharpening	0.0376	0.0445	0.0225	0.0445	0.0994	0.0505	0.0273	0.0456	0.2024	0.0519	0.0449	0.0462
JPEG 90	0	0.0381	0.0264	0.0381	0	0.0267	0.0233	0.0366	0	0.0361	0.0313	0.0408
70	0.0004	0.0555	0.0400	0.0555	0.0015	0.0614	0.0254	0.0559	0.0095	0.0613	0.0195	0.0604
50	0.0208	0.0766	0.0334	0.0880	0.0300	0.0750	0.0244	0.0858	0.0491	0.0801	0.0203	0.0894
40	0.0400	0.0952	0.0322	0.1090	0.0508	0.0955	0.0258	0.0985	0.0908	0.0934	0.0402	0.1016
30	0.0898	0.1011	0.0321	0.1271	0.1113	0.1140	0.0283	0.11507	0.1470	0.1105	0.0322	0.1127
Histogram equalization	0.0002	0.0470	0.0306	0.0047	0.0105	0.0359	0.0469	0.0206	0.0009	0.0429	0.0098	0.0427
Image blurring	0.0059	0.0312	0.0400	0.0312	0.0188	0.0419	0.0273	0.0354	0.0554	0.0745	0.0107	0.0685
Light increasing	0	0.0603	0.0244	0.0247	0.0012	0.0540	0.0186	0.0163	0.0007	0.0487	0.0117	0.0297
Light lowering	0	0.0725	0.0283	0.0066	0.0012	0.0712	0.0223	0.0220	0.0004	0.0786	0.0203	0.0723
Contrast increasing	0	0.0649	0.0205	0.0230	0.0007	0.0718	0.0576	0.0123	0	0.0690	0.0322	0.0256
Contrast lowering	0	0.0858	0.0229	0.0105	0.0004	0.0850	0.0352	0.0101	0	0.0795	0.0322	0.0216
Salt and peppers noise (0.01)+Gaussian filtering (3 × 3)	0.0081	0.1131	0.0205	0.0508	0.0203	0.1050	0.0195	0.0883	0.0371	0.0828	0.0078	0.0903
Median filtering (3 × 3) JPEG 70	0.0652	0.0958	0.0273	0.0795	0.1174	0.0877	0.0218	0.07621	0.1919	0.1180	0.0225	0.0721
Salt and peppers noise (0.01)+Gaussian filtering (3 × 3)+JPEG 70	0.0610	0.1276	0.0411	0.0938	0.0828	0.1304	0.0302	0.0920	0.1128	0.1403	0.0467	0.0936

**Table 7**

The watermark detection results for geometric distortions (BER).

Attacks	Lena				Barbara				Mandrill			
	Proposed scheme	Scheme in Chou and Liu (2010)	Scheme in Niu et al. (2011)	Scheme in Tsui et al. (2008)	Proposed scheme	Scheme in Chou and Liu (2010)	Scheme in Niu et al. (2011)	Scheme in Tsui et al. (2008)	Proposed scheme	Scheme in Chou and Liu (2010)	Scheme in Niu et al. (2011)	Scheme in Tsui et al. (2008)
<b>Rotation</b>												
5°	0.0029	N/A	0.0303	N/A	0.0142	N/A	0.0254	N/A	0.0557	N/A	0.0127	N/A
15°	0.0088	N/A	0.0371	N/A	0.0217	N/A	0.0276	N/A	0.0857	N/A	0.0223	N/A
45°	0.0154	N/A	0.0342	N/A	0.0273	N/A	0.0244	N/A	0.1008	N/A	0.0164	N/A
70°	0.0110	N/A	0.0283	N/A	0.0220	N/A	0.1074	N/A	0.0894	N/A	0.0127	N/A
90°	0	N/A	0.0309	N/A	0	N/A	0.0283	N/A	0	N/A	0.0225	N/A
<b>Scaling</b>												
0.5	0.0745	0.0402	0.0332	0.0501	0.1211	0.0693	0.0352	0.0583	0.2427	0.0593	0.0127	0.0577
0.9	0.0083	0.0247	0.0291	0.0359	0.0273	0.0383	0.0209	0.0359	0.1055	0.0386	0.0088	0.0348
1.2	0.0046	0.0216	0.0325	0.0336	0.0225	0.0284	0.0215	0.0401	0.0930	0.0279	0.0166	0.0356
1.5	0.0051	0.0374	0.0282	0.0412	0.0222	0.0255	0.0313	0.0440	0.0964	0.0284	0.0127	0.0352
2	0.0044	0.0102	0.0273	0.0484	0.0215	0.0336	0.0303	0.0502	0.0964	0.0347	0.0137	0.0510
<b>Translation</b>												
(H 2,V 15)	0	N/A	0.0283	N/A	0	N/A	0.0264	N/A	0	N/A	0.0146	N/A
(H 20,V 20)	0	N/A	0.0264	N/A	0	N/A	0.0186	N/A	0	N/A	0.0158	N/A
(H 15,V 2)	0	N/A	0.0322	N/A	0	N/A	0.0281	N/A	0	N/A	0.0176	N/A
(H 50,v0)	0	N/A	0.0244	N/A	0	N/A	0.0235	N/A	0	N/A	0.0156	N/A
(H 0,V 50)	0	N/A	0.0215	N/A	0	N/A	0.0234	N/A	0	N/A	0.0146	N/A
<b>Cropping</b>												
Centered cropping 10% off	0	0.0211	0.2100	0.0811	0	0.0271	0.1152	0.1660	0	0.0254	0.1406	0.1318
Centered cropping 20% off	0	0.0587	0.3662	0.1387	0	0.0691	0.3281	0.2188	0	0.0589	0.3633	0.1973
Centered cropping 30% off	0	0.0712	0.5039	0.2256	0	0.0845	0.4441	0.2451	0	0.0859	0.4268	0.2168
(H 10%, V 10%)	0	0.0812	0.0781	N/A	0	0.1238	0.1230	N/A	0	0.0825	0.0684	N/A
(H 20%, V 20%)	0	0.0960	0.1025	N/A	0	0.1318	0.1367	N/A	0	0.1066	0.0977	N/A
(H 30%, V 30%)	0	0.1221	0.1250	N/A	0	0.1360	0.1484	N/A	0	0.1275	0.1689	N/A
(H 50%, V 50%)	0	0.1434	0.4365	N/A	0	0.1515	0.4873	N/A	0	0.1472	0.4570	N/A
(H 60%, V 60%)	0.0352	0.1680	0.4986	N/A	0.0352	0.2074	0.5082	N/A	0.0352	0.1903	0.5018	N/A
<b>Length-width ratio change</b>												
(0.8,1,0)	0	N/A	0.0273	N/A	0.0017	N/A	0.0244	N/A	0.0464	N/A	0.0176	N/A
(0.9,1,0)	0.0004	N/A	0.0352	N/A	0.0054	N/A	0.0254	N/A	0.0151	N/A	0.0215	N/A
(1.1,1,0)	0.0002	N/A	0.0205	N/A	0.0054	N/A	0.0283	N/A	0.0206	N/A	0.0156	N/A
(1.2,1,0)	0.0007	N/A	0.0244	N/A	0.0059	N/A	0.0244	N/A	0.0251	N/A	0.0166	N/A
(1.0,0.8)	0.0015	N/A	0.0276	N/A	0.0085	N/A	0.0283	N/A	0.0342	N/A	0.0178	N/A
Scaling 2.0 + translation (H 0,V 15)	0.0046	N/A	0.0889	N/A	0.0215	N/A	0.1211	N/A	0.0974	N/A	0.0508	N/A
Rotation 45° + translation (H 20,V 20)	0.0420	N/A	0.0732	N/A	0.0552	N/A	0.1162	N/A	0.1294	N/A	0.0361	N/A
Scaling 0.9 + translation (H 5,V 15)	0.0122	N/A	0.1084	N/A	0.0293	N/A	0.1123	N/A	0.0627	N/A	0.0430	N/A
Scaling 1.2 + translation (H 5,V 15)	0.0061	N/A	0.0752	N/A	0.0234	N/A	0.1025	N/A	0.1021	N/A	0.0508	N/A
Translation (H 5,V 15) + salt and peppers noise (0.01)	0.0166	0.2315	0.1006	0.0785	0.0181	0.2451	0.1152	0.0663	0.0134	0.2484	0.0479	0.0737
Translation (H 20,V 20) + Gaussian filtering (3 × 3)	0.0029	N/A	0.1240	N/A	0.0046	N/A	0.1123	N/A	0.0217	N/A	0.0566	N/A

- has high computational complexity for SVR training, NSCT transform and image normalization.
- The multidimensional Fourier transform based color image watermarking scheme (Tsui et al., 2008): This nonblind color image watermarking scheme has low computational complexity. But, it has low watermark imperceptibility, because it does not modify the symmetric multidimensional Fourier transform coefficients. In addition, this scheme is fragile to some geometric distortions, including rotation, translation, and length-width ratio change. The underlying reason is that it also ignores the watermark desynchronization.

In sum, the experimental results demonstrate the proposed color image watermarking algorithm is robust to most common image processing operations (including color attacks) and geometric distortions, because the efficient pseudo-Zernike moments based LS-SVM geometric correction is utilized, whereas the imperceptibility is also maximized due to the reason that the symmetric quaternion Fourier transform coefficients are modified.

## 8. Conclusion

The existing color image watermarking schemes were always designed to mark the image luminance component only, which are sensitive to color attacks and geometric distortion. In this paper, we have proposed a blind color watermarking method in quaternion Fourier transform domain. The method embeds the watermark information into original color image by adaptively modulating the real coefficients of quaternion Fourier transform. For watermark decoding, the LS-SVM correction with pseudo-Zernike moments is utilized. Extensive experiments have indicated that the proposed watermarking method resists to a host of attacks significantly better than its competitors in the multiplicative watermark category.

Drawbacks of the proposed color image watermarking scheme are related to the computation time for LS-SVM training and pseudo-Zernike moments computation. Future work will focus on eliminating these drawbacks. In addition, to extend the proposed idea to color video watermarking is another future work.

## Acknowledgements

This work was supported by the National Natural Science Foundation of China under Grant Nos. 61272416, 60773031 & 60873222, the Open Foundation of State Key Laboratory of Information Security of China under Grant No. 04-06-1, the Open Foundation of Network and Data Security Key Laboratory of Sichuan Province, the Open Foundation of Key Laboratory of Modern Acoustics Nanjing University under Grant No. 08-02, and Liaoning Research Project for Institutions of Higher Education of China under Grant Nos. 2008351 & L2010230.

## References

- Barni, M., 2005. Effectiveness of exhaustive search and template matching against watermark desynchronization. *IEEE Signal Processing Letters* 12 (2), 158–161.
- Benhocine, A., Laouamer, L., Nana, L., Pascu, A., 2008. A new approach against color attacks of watermarked images. In: The 4th International Conference on Intelligent Information Hiding and Multimedia Signal Processing (IIH-MSP 2008), Harbin, China, 15–17 August 2008, pp. 969–972.
- Cheddad, A., Condell, J., Curran, K., 2010. Digital image steganography: survey and analysis of current methods. *Signal Processing* 90 (3), 727–752.
- Chou, C.H., Liu, K.C., 2010. A perceptually tuned watermarking scheme for color images. *IEEE Transactions on Image Processing* 19 (11), 2966–2982.
- Dejey, D., Rajesh, R.S., 2011. Robust discrete wavelet-fan beam transforms-based colour image watermarking. *IET Image Processing* 5 (4), 315–322.
- Deng, C., Gao, X., 2010. Local histogram based geometric invariant image watermarking. *Signal Processing* 90 (12), 3256–3264.
- Deng, C., Gao, X., Li, X., Tao, D., 2009. A local Tchebichef moments-based robust image watermarking. *Signal Processing* 89 (8), 1531–1539.
- Findik, O., Babaoglu, I., Ülker, E., 2011. A color image watermarking scheme based on artificial immune recognition system. *Expert Systems with Applications* 38 (3), 1942–1946.
- Fu, Y.G., Shen, R.M., 2008. Color image watermarking scheme based on linear discriminant analysis. *Computer Standard & Interfaces* 30 (3), 115–120.
- Gao, X.B., Deng, C., Li, X.L., 2010. Geometric distortion insensitive image watermarking in affine covariant regions. *IEEE Transactions on Systems, Man, and Cybernetics, Part C: Applications and Reviews* 40 (3), 278–286.
- Hazem, M., Sulaiman, S., 2011. Color image watermarking based on self-embedded color permissibility with preserved high image quality and enhanced robustness. *International Journal of Electronics and Communications* 65 (7), 619–629.
- Huang, H.Y., Yang, C.H., Hsu, W.H., 2010. A video watermarking technique based on pseudo-3D DCT and quantization index modulation. *IEEE Transactions on Information Forensics and Security* 5 (4), 625–637.
- Jiang, S., Hao, M., Zhang, J., Hu, B., 2008. Novel algorithms for fast hypercomplex Fourier transform and hypercomplex correlation with applications. *Acta Electronica Sinica* 36 (1), 100–105.
- Jung, S.-W., Ha, L.T., Ko, S.-J., 2011. A new histogram modification based reversible data hiding algorithm considering the human visual system. *IEEE Signal Processing Letters* 18 (2), 95–98.
- Kang, X., Huang, J., Zeng, W., 2010. Efficient general print-scanning resilient data hiding based on uniform log-polar mapping. *IEEE Transactions on Information Forensics & Security* 5 (1), 1–12.
- Kaur, M., Kaur, P., 2009. Robust watermarking into the color models based on the synchronization template. In: International Conference on Information and Multimedia Technology (ICIMT '09), Jeju, Island, 16–18 Dec, 2009, pp. 296–300.
- Khotanzad, A., Hong, Y.H., 1990. Invariant image recognition by Zernike moments. *IEEE Transactions on Pattern Analysis and Machine Intelligence* 12 (5), 489–497.
- Kumar, A., Santhi, V., 2011. A review on geometric invariant digital image watermarking techniques. *International Journal of Computer Applications* 12 (9), 31–36.
- Li, L., Qian, J., Pan, J., 2011. Characteristic region based watermark embedding with RST invariance and high capacity. *International Journal of Electronics and Communications* 65 (5), 435–442.
- Lin, Y.T., Huang, C.Y., Lee, G.C., 2011. Rotation, scaling, and translation resilient watermarking for images. *IET Image Processing* 5 (4), 328–340.
- Liu, K.-C., 2010. Wavelet-based watermarking for color images through visual masking. *AEU – International Journal of Electronics and Communications* 64 (2), 112–124.
- Liu, J., Huang, H., 2008. A digital watermarking algorithm for color images using image correction. *Proceedings of SPIE* 7125, 71251D.
- Liu, Y., Zheng, D., Zhao, J., 2007. An image rectification scheme and its applications in RST invariant digital image watermarking. *Multimedia Tools and Applications* 34 (1), 57–84.
- Moxey, C., Sangwine, S., Ell, T., 2002. Color-grayscale image registration using hypercomplex phase correlation. *Proceedings of the 2002 IEEE International Conference on Image Processing* 3, 247–250.
- Muhammad, K.K., 2011. Research advances in data hiding for multimedia security. *Multimedia Tools and Applications* 52 (2–3), 257–261.
- Nian, G., Tang, X., Wang, D., 2010. Geometric distortions correction scheme based on Hausdorff distance for digital watermarking image. *The Second International Conference on MultiMedia and Information Technology* 2, 43–46.
- Niu, P.P., Wang, X.Y., Yang, Y.P., Lu, M.Y., 2011. A novel color image watermarking scheme in nonsampled contourlet-domain. *Expert Systems with Applications* 38 (3), 2081–2098.
- Pei, S., Ding, J., Chang, J., 2001. Efficient implementation of quaternion Fourier transform, convolution, and correlation by 2-D complex FFT. *IEEE Transactions on Signal Processing* 49 (11), 2783–2797.
- Peng, H., Wang, J., Wang, W.X., 2010. Image watermarking method in multiwavelet domain based on support vector machines. *Journal of Systems and Software* 83 (8), 1470–1477.
- Qiu, Y., Lu, H., Deng, N., Cai, N., 2011. A robust blind image watermarking scheme based on template in Lab color space. *Communications in Computer and Information Science* 234, 402–410.
- Rastegar, S., Namazi, F., Yaghmaie, K., Aliabadian, A., 2011. Hybrid watermarking algorithm based on singular value decomposition and radon transform. *International Journal of Electronics and Communications* 65 (7), 658–663.
- Sadasivam, S., Moulin, P., Coleman, T.P., 2011. A message-passing approach to combating desynchronization attacks. *IEEE Transactions on Information Forensics and Security* 6 (1), 894–905.
- Sangwine, S., Ell, T., 2001. Hypercomplex Fourier transforms of color images. *Proceedings of the 2002 IEEE International Conference on Image Processing* 1, 137–140.
- Seo, J.S., Yoo, C.D., 2006. Image watermarking based on invariant regions of scale-space representation. *IEEE Transactions on Signal Processing* 54 (4), 1537–1549.
- Singhal, A., Singh, R.P., Tenguria, M., 2011. Comparison of different wavelets for watermarking of colored images. In: The 3rd International Conference on Electronics Computer Technology, Kanyakumari, 8–10 April 2011, pp. 187–191.
- Todd, A.E., Stephen, J.S., 2007. Hypercomplex Fourier transforms of color images. *IEEE Transactions on Image Processing* 16 (1), 22–35.
- Tsai, H.H., Sun, D.W., 2007. Color image watermark extraction based on support vector machines. *Information Sciences* 177 (2), 550–569.
- Tsai, J.-S., Huang, W.-B., Kuo, Y.-H., 2011. On the selection of optimal feature region set for robust digital image watermarking. *IEEE Transactions on Image Processing* 20 (3), 735–743.

- Tsui, T.K., Zhang, X.-P., Androullos, D., 2008. Color image watermarking using multidimensional Fourier transforms. *IEEE Transactions on Information Forensics and Security* 3 (1), 16–28.
- Valizadeh, A., Wang, Z.J., 2011. Correlation-and-bit-aware spread spectrum embedding for data hiding. *IEEE Transactions on Information Forensics and Security* 6 (2), 267–282.
- Vapnik, V., 1995. *The Nature of Statistical Learning Theory*. New York, Springer-Verlag.
- Wang, X.-Y., Hou, L.-M., 2010. A new robust digital image watermarking based on pseudo-Zernike moments. *Multidimensional Systems and Signal Processing* 21 (2), 179–219.
- Wang, X., Wu, J., Niu, P., 2007. A new digital image watermarking algorithm resilient to desynchronization attacks. *IEEE Transactions on Information Forensics and Security* 2 (4), 655–663.
- Wang, X.-Y., Xu, Z.-H., Yang, H.-Y., 2009. A robust image watermarking algorithm using SVR detection. *Expert Systems with Applications* 36 (5), 9056–9064.
- Wang, X.-Y., Niu, P.-P., Meng, L., Yang, H.-Y., 2011. A robust content based image watermarking using local invariant histogram. *Multimedia Tools and Applications* 54 (2), 341–363.
- Wu, J., 2009. A RST invariant watermarking scheme utilizing support vector machine and image moments for synchronization. In: 2009 Fifth International Conference on Information Assurance and Security, Xi' An, China, pp. 572–574.
- Zhang, H., Shu, H., Gouenou, C., 2011. Affine Legendre moment invariants for image watermarking robust to geometric distortions. *IEEE Transactions on Image Processing* 20 (8), 2189–2199.
- Zheng, J.B., Feng, S., 2009. A color image watermarking scheme in the associated domain of DWT and DCT domains based on multi-channel watermarking framework. In: IWDW 2008, LNCS 5450. Springer, pp. 419–432.
- Zheng, D., Liu, Y., Zhao, J., 2007. A survey of RST invariant image watermarking algorithms. *ACM Computing Surveys* 39 (2), 1–91.
- Xiang-yang Wang** is currently a Professor with the Multimedia and Information Security Laboratory, School of Computer and Information Technology, Liaoning Normal University, China. His research interests lie in the areas of information security, image processing, pattern recognition, and computer vision. He is the author of two books. He has published over 100 papers in international journals (including IEEE T SIGNAL PROCES, IEEE T AUDIO SPEECH, IEEE T INF FOREN SEC, IEEE MULTIMEDIA, PATTERN RECOGN, J VIS COMMUN IMAGE R, SIGNAL PROCESS etc.) and 25 papers in international conferences and workshops. Mr. Wang is a Reviewer for many leading international and national journals and conferences, including IEEE Trans. and IEE Trans. etc.
- Chun-peng Wang** received the B. E. degree from the School of Computer and Information Technology, Liaoning Normal University, China, in 2010, where he is currently pursuing the M. S. E. degree. His research interests include image watermarking and signal processing.
- Hong-ying Yang** is currently a professor with the School of Computer and Information Technology at the Liaoning Normal University, China. She received her B. E. degree from the Liaoning Normal University, China and her M. S. E. degree from the Dalian Maritime University, China, in 1989 and 2010, respectively. Her research interests include signal processing and communications, digital multimedia data hiding.
- Pan-pan Niu** received the B. E. degree and M. S. E. degree from the School of Computer and Information Technology, Liaoning Normal University, China, in 2006 and 2009, respectively, where she is currently pursuing the Ph.D. degree. Her research interests include image watermarking and signal processing.